UNMANNED AERIAL SYSTEM INSPECTION OF

INSTRUMENT LANDING SYSTEM

RADIO SIGNALS

By

JOSEPH JANTZ

Bachelor of Science in Electrical Engineering
Oklahoma State University
Stillwater, Oklahoma
2017

Submitted to the Faculty of the
Graduate College of the
Oklahoma State University
in partial fulfillment of
the requirements for
the Degree of
MASTER OF SCIENCE
May 2019

UNMANNED AERIAL SYSTEM INSPECTION OF

INSTRUMENT LANDING SYSTEM

RADIO SIGNALS

Thesis Approved:

Dr. Jim West

Thesis Adviser

Dr. Chuck Bunting

Dr. Sabit Ekin

ACKNOWLEDGEMENTS

I would like to thank Drs. Jim West, Chuck Bunting, and Sabit Ekin for the education and mentorship they gave me while in graduate school. I would also like to thank OSU's USRI and the FAA Flight Inspection Group for supporting the project that allowed me to write this thesis. Final thanks go to my friends Mr. Daniel Smith, Jeff Reinecke, Big John Williams, Marshal Dilley, and Zach Amon for encouraging me and keeping me entertained through seven years of engineering school.

Acknowledgements reflect the views of the author and are not endorsed by committee members of Oklahoma State University.

Name: JOSEPH JANTZ

Date of Degree: MAY 2019

Title of Study: UNMANNED AERIAL SYSTEM INPECTION OF INSTRUMENT LANDING SYSTEM RADIO SIGNALS

Major Field: ELECTRICAL ENGINEERING

Abstract: This study investigates the use of a unmanned aerial system (UAS) for instrument landing system (ILS) signal inspection. A model of expected equivalent isotropic receiver power was built. A 10-meter radio tower was constructed to be used as the test ILS source. Then, empirical channel power measurements were made with antennas and a spectrum analyzer mounted on the prototype vehicle in a simulated ILS environment. Channel power measurements were made by the prototype UAS at various altitudes 19.4 km (12.1 miles) from the base station. Comparisons are made between model and empirical data. The model reasonably predicted signal level and lobing patterns for two of the three ILS component signals. A method of channel power correction based on aircraft orientation was attempted but was ineffective due to UAS pitch data suspected to be inaccurate. This study finds that signal level inspection of ILS can be done by UAS with a reasonable level of repeatability and that measurement accuracies of ±1.0 dB and ±1.5 dB were achievable for localizer and glideslope respectively. Larger changes in signal levels can be observed on a day-to-day basis. This is likely due to changing atmospheric conditions and tear-down and reassembly of the base station.

TABLE OF CONTENTS

Chapter Page

LIST OF TABLES

Table Page

LIST OF FIGURES

Figure Page

Figure Page

CHAPTER I

INTRODUCTION

An Instrument Landing System (ILS) is a radio air navigation system broadcast from an airport utilized by airplanes approaching a runway. This set of radio signals provides information that describes the position of the aircraft relative to the target runway along the aircraft's path of approach. ILS does not directly track the position of the aircraft and relay this information to the aircraft. Instead, the antenna arrays project a target approach path for the aircraft to track. Distance from the runway is found by the aircraft pinging the ILS and determining distance based on return delay. The information is displayed on instrument gauges familiar to pilots. This system acts as a supplementary instrument that guarantees smoother, more accurate landings as well as a crutch for fixed-wing aircraft landing in low visibility weather conditions. The three principal signals composing ILS, localizer (LOC), glideslope (GS), and distance measurement equipment (DME), are described below.

Localizer is the signal that the aircraft follows for horizontal positioning information and indicates whether the aircraft is on track to land right or left of the runway's center line. The aircraft works out the horizontal position relative to runway center by measuring the depth of modulation of the received localizer signal. Receiving a prominent modulation of 90 Hz indicates the aircraft is left of center, while a prominent modulation of 150 Hz indicates the

aircraft is right of center. There are forty available localizer channels available for use between 108.0-117.975 MHz [1].

Glideslope functions similarly to localizer, referencing vertical position relative to a target sloped plane indicating the slope the aircraft is meant to follow during approach. Receiving a prominent modulation of 90 Hz indicates the aircraft is above the target path, while a prominent modulation of 150 Hz indicates the aircraft is below the target path. The intersection of the vertically oriented localizer target plane and the sloped glideslope plane form a target path for the aircraft to follow. Glideslope channel allocation is 328.6-335.4 MHz [1].

Distance measuring equipment (DME), as the name implies, allows the pilot to determine the distance from aircraft to runway. The DME measurement represents the distance along the slopped path to the edge of the runway and should not be assumed to be the ground distance from runway. As mentioned previously, this aircraft tool works by pinging the ILS and deriving the distance from the echoed signal's delay. DME allocation is 1025-1150 MHz [1].

These valuable systems are inspected by the Federal Aviation Administration (FAA) of the United States for accuracy and range. The signals are assessed by air navigation analyzers on board manned aircrafts flying patterns in range of the runways. The cost of owning and maintaining a fleet of inspection aircraft, as well as employing pilots and data-interpreting engineers, is large. This creates a large monetary incentive for the development of a smaller unmanned inspection aircraft operable by a trained technician. The implementation of unmanned ISL inspection systems could also save time, allow for more frequent inspection of ILS, and increase the accuracy of measurements. The current manned system is suspected to contain large errors in measurements due to aircraft inference. To help progress this idea the FAA started a joint prototype development project in 2017 with the Unmanned Systems Research Institute (USRI) of Oklahoma State University (OSU) with support of OSU's Robust Electromagnetic

Field Testing and Simulation (REFTAS) group. These groups set out to prove a UAS protype by measuring strictly signal power levels received from a simulated ILS. This thesis stems from field data collected during this project.

This thesis describes the unmanned aerial system (UAS) developed, the field-testing process of the UAS, model of expected electromagnetic field power for the test location, electromagnetic field power profiles collected in-field, comparisons of model and empirical data, and potential measurement correction methods.

Chapter 2 describes the unmanned aircraft developed, base station for simulating the ILS sources, and the field test location. Chapter 3 contains a model meant to predict electromagnetic power received by the unmanned aircraft. The purpose of this model is to help determine necessary simulated ILS transmission powers for test purposes without speculation and to have a metric to which compare empirical data. Chapter 4 presents electromagnetic power data from field test measurements and comparisons are made to model data. Chapter 5 features a method of correcting measurement profiles based on aircraft orientation at the time of discrete power measurement. Chapter 6 will contain the conclusion.

CHAPTER II

VEHICLE, BASE STATION, AND LOCATION

To develop a UAS capable of measuring ILS signal strength, it is important to test the device in a real-world setting. Target specifications for such a device would include the capabilities to capture an ILS signal at as high an altitude as 1600 ft (488 m) above ground level (AGL), miles from the transmission source. This testing would ideally be done near an airport, but because of potential interference with everyday airport operations it was necessary that a simulated environment be created. The test setup for in-field measurements consists of the UAS itself, as well as a simulated ILS source and reasonably flat location to contain the experiment.

2.1 – EQUIPMENT LIST

Vehicle:

- Rhodes & Schwarz FSH8 Spectrum Analyzer
- Rhodes & Schwarz EVS-Z3 ILS/VOR Dipole Antenna Set
- Custom 1155 GHz Monopole Antenna with Ground-Plane
- BFD Systems GD-40X UAS

Base Station:

- BlueSky Mast AL1
- GBAS VHF Dipole TX FA60.20A-014
- Kathrein Model SCA-CA5-120/HCM (VOR/LOC Yagi-Uda)
- RFI Wireless RDA6-99 (GS TX Antenna)
- (1) Log-Periodic Antenna (DME)
- (3) Pasternak RF Cables (N type-M/M type-N) (various lengths)
- [Generators/Amps]
    - Localizer: R&S SMBV100A Signal Generator, EIN Model 411LA VHF RF Amplifier
    - Glideslope: R&S SMA100A Signal Generator, Crescend PM1-525-10 RF Amplifier
    - DME: R&S SMA100B Signal Generator (High-Power Option)

2.2 – VEHICLE

A multirotor aircraft is advantageous for radio signal inspection. It allows the measuring equipment to be hovered in three-dimensional space with a desired heading. Because of the weight of the antenna and signal analyzing equipment, a large multirotor is required. The selection and assembly of remote multirotor components was accomplished by the USRI of OSU.

A semi-custom GD-40X UAS was ordered from BFD Systems. The GD-40X is a multirotor with 4 pairs of motors capable of carrying larger payloads than most consumer multirotors (50 lbs.). The UAS is approximately 71 cm tall and 86 cm wide with 70 cm props. The USRI designed and manufactured a carbon plate assembly that held the measuring equipment to the UAS. Using a DJI brand flight controller, the team was able to program complex flight paths comprised of discrete positions capable of sending trigger signals to the measurement instrument. This enabled the flight paths described in chapter 4.

Figure 2.2.1 - GD-40X UAS with mounted measurement equipment

The instrument used in these experiments to determine radio signal strength is the Rhode & Schwarz (R&S) FSH8 spectrum analyzer. A FSH8 was loaned by the FAA to OSU for this project. This spectrum analyzer is advantageous because of its light weight. The FSH8 is a handheld model that weighs less than 6.6 lbs. [2].

Custom setting states for the FSH8 were created based on ILS signals tested. The states were made to measure channel power over an appropriate bandwidth of integration and centered on the broadcasted frequency. The channel bandwidths were made wide enough for each state to capture all signal power, but not too large to avoid capturing noise. True localizer and glideslope signals were broadcast, while DME was broadcast as a "dummy" or simulated continuous waveform source from the base station. The DME center frequency was chosen based on the band allocation mentioned in chapter 1.

The FSH8 also has a trigger port that was utilized to trigger spectrum analyzer sweeps. Upon sweeps, the FSH8 captures the channel power measurement and saves the data to external memory. The measurements are retrieved after each flight. The trigger signal comes from the flight controller on the UAS. The triggers occur at the defined flight positions in the flight path. This allowed for the creation of an automated flight and measurement triggering system.

The antennas used to receive the ILS signals on the UAS were the R&S EVS-Z3 ILS/VOR Dipole Set and a custom built 1155 MHz monopole with a circular, half-wavelength diameter ground-plane. The antennas mount to the underside of the UAS on the carbon fiber payload structure and are connected to the FSH8 by a short RF cable.

The EVS-Z3 Dipole Set contains two separate half-wave dipoles used for the horizontally-polarized glideslope and localizer. Naturally, the shorter dipole is for glideslope and the longer for localizer.

A custom monopole was built to receive the vertically-polarized DME signal. The finite-radius ground plane causes the antenna to have a direction of maximum gain at a non-perpendicular angle to the element. This can be advantageous over a standard monopole if the incident wave is at a slight grazing angle relative to the plane of maximum gain for a standard dipole. As will later be shown, this is the case for this experiment.

The monopole ground plane was cut from 0.09” sheet aluminum by a CNC cutter. The monopole element was cut from a longer whip antenna. It was cut slightly longer than a quarter wavelength (7 cm). The element was driven into a female BNC connector that was attached to the ground plane. The antenna was then tuned in an anechoic chamber with a vector network analyzer (VNA). Using S-parameter S_{11} the frequency of least power return can be found. Because the element was cut longer than necessary, the antenna was tuned by incrementally trimming the element to bring the frequency of least return up to 1155 MHz.

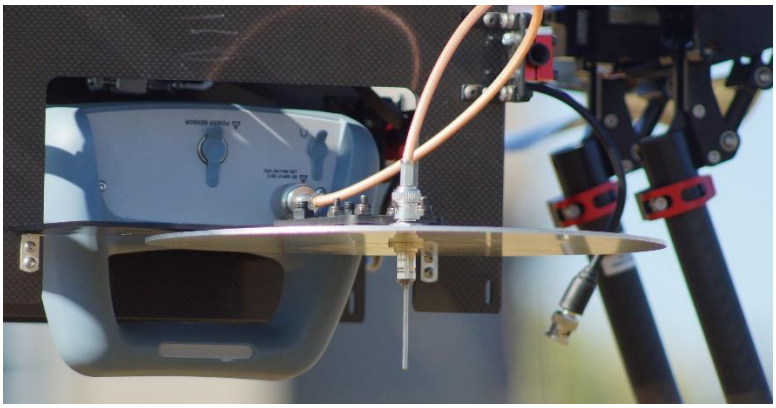

Figure 2.2.2 - Monopole antenna with ground plane on UAS

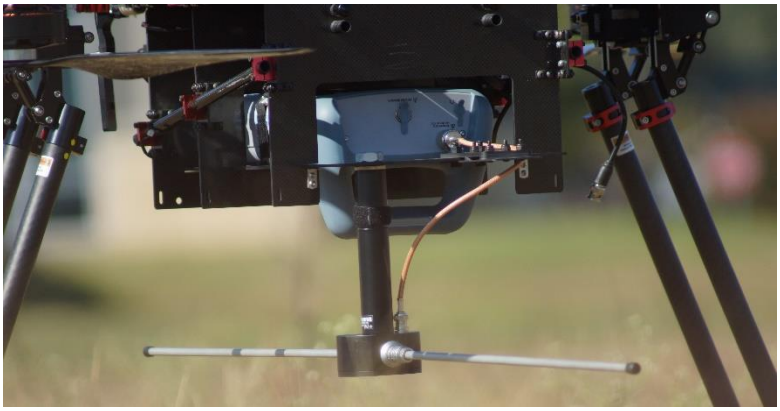

Figure 2.2.3 - Localizer dipole antenna on UAS

Figure 2.2.4 - Glideslope dipole antenna on UAS

2.3 – BASE STATION

The base station is responsible for generating, amplifying, and transmitting the simulated ILS signals for the experiment. It consists of a 10-meter BlueSky mast, signal generators, amplifiers, and antennas for each signal. Localizer is transmitted by a 5-element Yagi-Uda array 5.5 meters up the mast, glideslope by a 6-element Yagi-Uda array at 8.6 meters, and DME by a log-periodic at 9.85 meters. The lowest antenna on the mast is an unused DME receiver. Antenna gain and generator/amp levels will be discussed section 3.2.

Figure 2.3.1 - Base station

2.4 – LOCATION

The Mike Monroney Aeronautical Center (MMAC) was chosen as the location for the base station. The FAA team working on this project were located nearby and had access to the facility. Additionally, MMAC's location was convenient because it lays on the outskirts of Oklahoma City, where it has a relatively clear propagation path to the surrounding rural area. Propagating into a rural area allows for more liberties when flying a UAS given the surplus of open space, lack of tall buildings, and generally lower airspace traffic and classifications. MMAC is on the southwest side of Oklahoma City.

A clear, flat field is the preferred location for operating unmanned multirotors for measurement purposes. The large amount of space makes launches and landings safer and easier. Tuttle High School (THS) in Tuttle, Oklahoma allowed us to set up UAS operations in the field north-east of their building. This location is directly south-west from the base station at MMAC and the land between locations is generally barren and relatively flat.

The MMAC base station is located at coordinates 35°23'11.64"N, 97°37'36.89"W at an altitude of 1280 ft (390 m) mean sea level (MSL). The UAS ground reference point was at coordinates 35°17'44.47"N, 97°48'32.81"W at an altitude of 1300 ft (396 m) MSL. The ILS signals are transmitted from MMAC and propagate south-west, away from Oklahoma City and towards Tuttle, to be received by the UAS.

Figures 2.4.1 and 2.4.2 bellow depict the path of propagation from MMAC to THS. Figure 2.4.1 is sourced from Google Maps Pro. It has satellite image of the region as well as elevation under the path. The elevation-under-path data from this figure can be used to verify similar data derived from United States Geological Survey (USGS) digital terrain elevation data (DTED) in the following chapter. Figure 2.4.2 was generated in MATLAB using USGS DTED for the region.

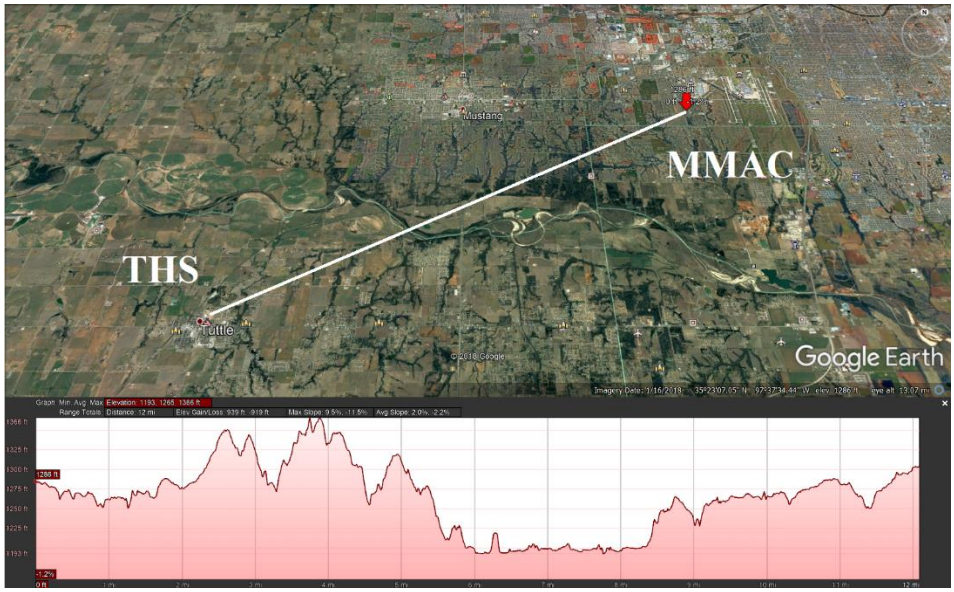

Figure 2.4.1 - Propagation path and elevation data from Google Earth Pro

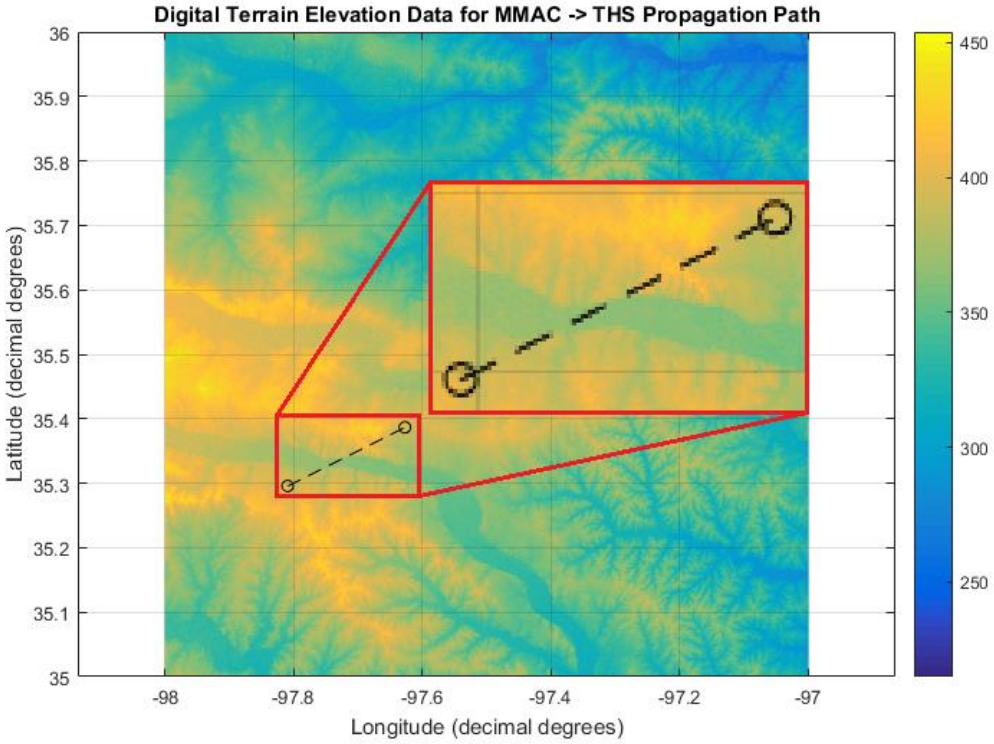

Figure 2.4.2 - Propagation path mapped on USGS DTED with zoom [Units: meters above sea level]

CHAPTER III

THEORETICAL MODEL OF EQUIVALENT ISOTROPIC RECIEVER POWER

To form a prediction of power the UAS will receive from the base station several geometric properties must be known and appropriate mechanisms of propagation must be applied. Useful geometries include transmitter and receiver heights as well as propagation distance and elevation under the propagation path. The mechanisms of propagation that govern this system are path loss, reflection, and refraction. In the sections following, all components will be combined to form a cohesive model of equivalent isotropic receiver power (EIRxP) based on UAS altitude above ground level (AGL).

3.1 – GEOMETRY

The refractive index of the atmosphere is not homogenous. The refractive index changes with altitude forming a refractive gradient. For low altitudes the refractivity can be approximated as linearly increasing. This approximately linear refractivity gradient causes radio waves to propagate in arcs instead of straight lines. The curvature of the propagated ray can be geometrically transformed into an effective earth curvature or radius. This model of changing the Earth's radius so that propagation rays can be represented as straight lines in a standard Earth atmosphere is the 4/3 Earth radius or straight-ray model [3].

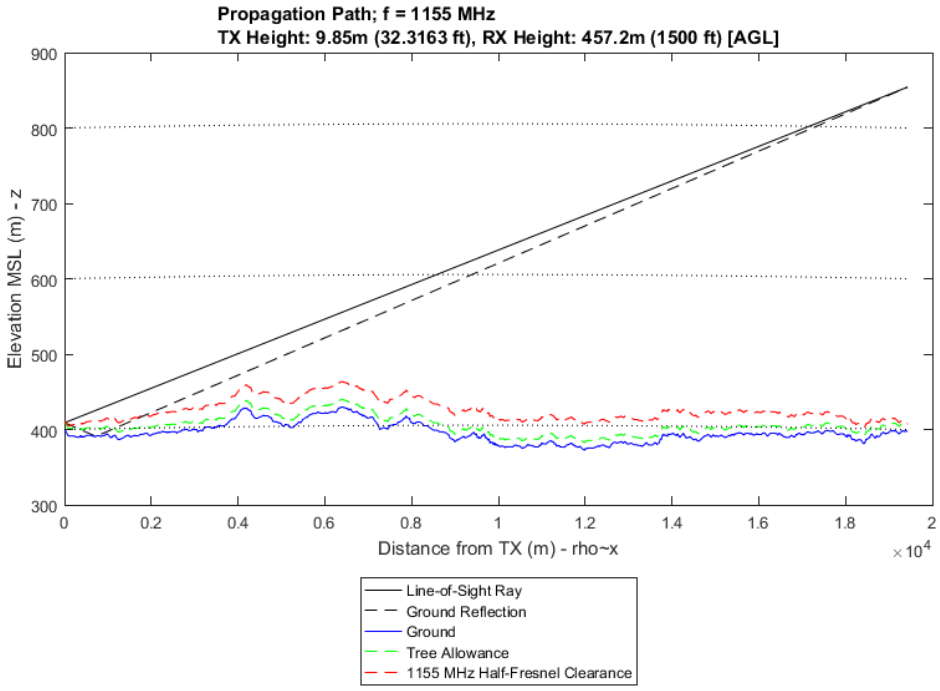

Figure 3.1.1 - Propagation paths for DME and elevation under rays

Figure 2.1.1 depicts the line-of-sight ray, ground reflection ray, elevation under rays, 10-meter tree clearance, and half Fresnel clearance. The half Fresnel clearance is incorporated to avoid diffraction effects from the ground. The ray lines are mapped over a 4/3 radius earth model, which is a model used to incorporate the refractivity gradient of a standard atmosphere into an effective earth radius. This allow for the rays to be depicted as straight lines by exaggerating the ground curvature. On the left side of the figure is the base station and on the right is the UAS at 1500 ft (457 m) AGL. The transmit antennas are at different heights from each signal. For this EIRP model we will focus on receiver heights between 500 and 1600 ft (152 and 488m) AGL, this encompasses the vertical region the UAS inspects during the experiment. The surface distance between the UAS ground reference point and base station coordinates is 12.07 miles (19.43 km). We start the calculations for this model with basic parameters for each signal.

Signal Name	Freq. Used, f	Wavelength, λ	Transmitter Height, h_{TX}
Localizer	108.0 MHz	2.776 m	5.5 m
Glideslope	334.7 MHz	0.8957 m	8.6 m
DME	1155 MHz	0.2596 m	9.85 m

Table 3.1.1 - Basic transmission parameters

With [4]

$$\lambda = \frac{c}{f} \ , \tag{3.1.1}$$

$$c = 2.998 \ \times 10^{8} \ {}^{\mathrm{m}}/_{\mathrm{s}} \, .$$

Receiver height for all signals are

$$500 \text{ ft} \ \leq \ h_{RX} \ \leq 1600 \text{ ft} \ \ or \ \ 152 \text{ m} \ \leq \ h_{RX} \ \leq 488 \text{ m}.$$

Surface distance between the UAS ground reference point and base station coordinates is

$$d = 19.43 \text{ km}.$$

The curvature of the surface in this 4/3 Earth radius model can be described as [5]

$$\text{curve}(\rho) = \frac{\left(\frac{d}{2}\right)^2 - \left(\frac{d}{2} - \rho\right)^2}{2a} \ , \tag{3.1.2}$$

where 'ρ' is the distance along the curve and 'a' is the effective Earth radius.

$$a = \frac{4}{3} \, r_E = \frac{4}{3} * 6.366 \times 10^6 m = 8.488 \times 10^6 m.$$

From this the curve at ρ = 0 and ρ = d is 0 m. The maximum curve height, or bulge, occurs at ρ = d/2 with a maximum curve height of 5.6 m.

3.2 – TRANSMITTER POWER

The following table shows the power output of the signal generator, the RF amplifier gain, and total transmitted power for each ILS signal. These are the levels used for all prototype field testing. The table also includes cable losses and power delivered to the antenna, P_{TX}. Cable losses are measured figures.

Signal	Generator Output, P_{out}	Amplifier Gain, G_A	Total, P_O	Cable Loss	P_{TX}
Localizer	-23.0 dBm	40.4 dB	17.4 dBm	1.4 dB	16.0 dBm
Glideslope	-26.0 dBm	43.0 dB	17.0 dBm	1.9 dB	15.1 dBm
DME	37.0 dBm	0.0 dB	37.0 dBm	3.8 dB	33.2 dBm

Table 3.2.1 - Transmitter power

3.3 – PATH LOSS

Path loss is the loss in signal power associated with the field power density decreasing over distance. Path loss can be calculated from [6]

$$\mathrm{PL_{dB}} = 20\log_{10}\left(\frac{\lambda}{4\pi d}\right). \tag{3.3.1}$$

The path loss calculated for each signal is in the table below.

Signal	Path Loss, PL_{dB}
Localizer	98.9 dB
Glideslope	108.7 dB
DME	119.5 dB

Table 3.3.1 - Path loss

3.4 – GROUND REFLECTION COEFFECIENT

The magnitude of the ground-reflected field that reaches the receiver is dependent on the reflection coefficient between air and ground. Ground reflection coefficients are [7]

$$\Gamma(\alpha) = \frac{\sin(\alpha) - \chi}{\sin(\alpha) + \chi} \tag{3.4.1}$$

Where ‘α’ is the grazing angle between the incident ray and ground and ‘X’ is a polarization-based term. X for each polarization is [7]

$$\chi_v = \frac{\sqrt{\epsilon_g - cos^2(\alpha)}}{\epsilon_g}, \tag{3.4.2}$$

$$\chi_h = \sqrt{\epsilon_g - cos^2(\alpha)}. \tag{3.4.3}$$

The relative complex ground permittivity ϵ_g was based on empirical ground dielectric constant and ground conductivity data was taken from a location in Oklahoma [8]. This data is more applicable to this specific scenario than empirical data taken from other regions or theoretically derived data. The complex ground relative permittivity is as follows [7]

$$\epsilon_g = \epsilon_r - j\frac{\sigma_g}{\epsilon_0 2\pi f}, \qquad (3.4.4)$$

$$\epsilon_r = 10 \quad , \quad \sigma_g = 0.1\,{}^{\mathrm{S}}/_{\mathrm{m}}.$$

The table below contains relative ground permittivity data for each ILS signal.

Signal	Relative Ground Permittivity, ϵ_g
Localizer	10 – j16.6
Glideslope	10 – j5.4
DME	10 – j1.6

Table 3.4.1 - Ground permittivity

Evaluating equation 3.4.1 over $0° \leq \alpha \leq 90°$ yields the following figures for ground reflection coefficients for vertical and horizontal polarizations.

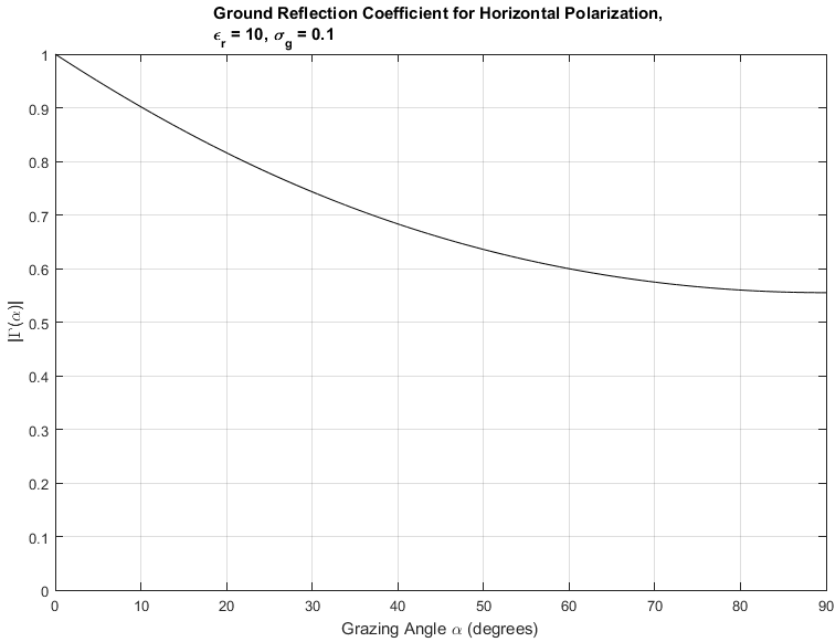

Figure 3.4.1 – Ground reflection coefficient for horizontal polarization

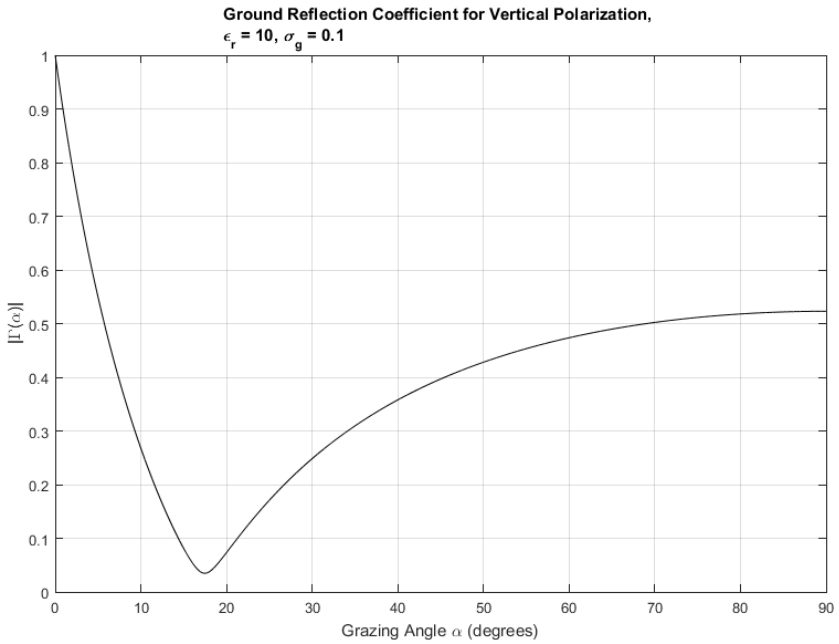

Figure 3.4.2 - Ground reflection coefficient for vertical polarization

3.5 – REFLECTION PATTERN

A reflection pattern (RP) describes the interference between the line-of-sight ray and the ground reflection ray. When working in a two-ray model, meaning only line-of-sight and primary ground reflection ray are considered, the maximum field strength gain is 2. The maximum power gain would then be 2^2 or 4, based on the square relationship between field and power. This means the maximum value of the reflection pattern, in decibels, is 6 dB. The minimum value would be - ∞ dB indicating completely destructive interference. To find the reflection pattern of the base station, the ground reflection can be modeled as having a source that is an image of the base station. The radiation pattern from this two-source system can then be derived from equations for the array factor (AF) of a two-element linear array. The figure below depicts the projection of the ground reflection as an image. Scattering and reflected-wave spreading due to Earth curvature will be discussed in the next section.

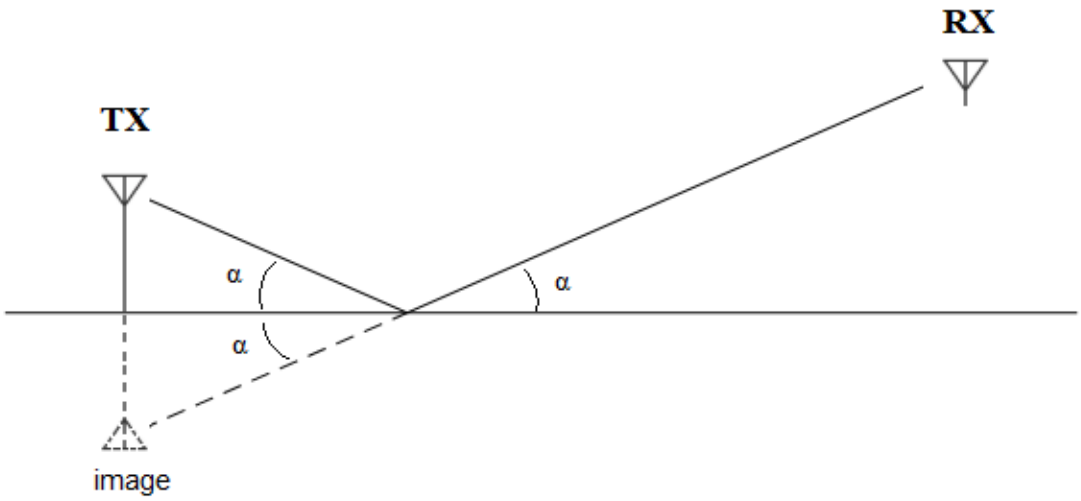

Figure 3.5.1 - Ground reflection projection

The array factor of a linear array is [9]

$$AF = \sum_{n=1}^{N} a_n e^{j(n-1)\Psi}, \tag{3.5.1a}$$

$$\Psi = kdcos(\gamma) + \beta, \tag{3.5.1b}$$

where a_n is the weight of the n^{th} element, N is the total number of elements, k is the wave number, d is the distance between elements, γ is the angle relative to the array axis, and β is the phase progression between elements.

Because the second element is an image, there is zero feed phase progression. The phase difference between the two signals at the receiver is derived from the difference in lengths of propagation paths, which is described by Ψ – β, and dielectric properties of the ground.

$$\beta = 0$$

In this theoretical model for EIRxP, the angle used (α) is in reference to the ground. At the launch point this is a 90° difference compared to the angle used in this AF equation (γ). A relationship between the two variables can be defined on the region $0° \leq \alpha \leq 90°$.

$$\alpha = \gamma + 90°,$$

$$\gamma = \alpha - 90°,$$

$$\cos(\gamma) = \cos(\alpha - 90°) = \sin(\alpha).$$

It is convenient to work the variables k and d as a single phase term [4]

$$k = \frac{2\pi}{\lambda}, \tag{3.5.2}$$

$$d = 2 * h_{TX},$$

$$kd = \frac{4\pi h_{TX}}{\lambda}. \tag{3.5.3}$$

Below is a table containing kd for each ILS signal.

Signal Name	Transmitter Height, h_{TX}	Wavelength, λ	kd
Localizer	5.5 m	2.776 m	24.90
Glideslope	8.6 m	0.8957 m	120.7
DME	9.85 m	0.2596 m	476.8

Table 3.5.1 - "kd" terms

The element weights in the array factor equation correspond to the fraction of the ray's power that reaches the receiver (ignoring path loss). The weight for the first element, the transmitter, is 1, meaning the line-of-sight ray encounters no obstacles on the path to the receiver. The weight for the second element represents the magnitude of the field reflected from the ground and the polarization of the reflected field relative to the line-of-sight ray. The reflected ray of a horizontally polarized field leaves the ground with the same polarization as the line-of-sight ray. For a vertically polarized field, the exiting polarization is inverted relative to the line-of-sight ray. This would be equivalent to a 180° phase shift.

For horizontally polarized localizer and glideslope

$$a_1 = 1 \text{ and } a_2 = \Gamma(\alpha).$$

For vertically polarized DME

$$a_1 = 1 \text{ and } a_2 = -\Gamma(\alpha).$$

Combining all this information to find the array factors yields

$$Horizontal\ Polarization\colon\ AF(\alpha) = 1 + \Gamma(\alpha)e^{\frac{j4\pi}{\lambda}h_{TX}\sin(\alpha)}, \tag{3.5.4a}$$

$$Vertical\ Polarization\colon\ AF(\alpha) = 1 - \Gamma(\alpha)e^{\frac{j4\pi}{\lambda}h_{TX}\sin(\alpha)}. \tag{3.5.4b}$$

Array factors describe the field strength magnitude based on transmission angle. The reflection pattern (RP) describes the power density based on transmission angle. The relationship between the two is

$$RP(\alpha) = |AF(\alpha)|^2, \tag{3.5.5}$$

and in dB

$$RP(\alpha)_{dB} = 20\log_{10}(|AF(\alpha)|). \tag{3.5.6}$$

Below are the polar plots for reflection patterns of each base station signal found using the last equation.

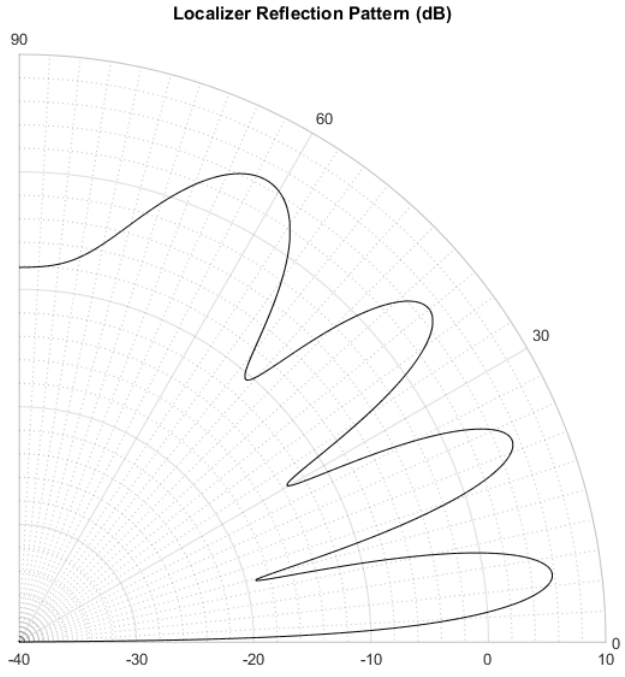

Figure 3.5.2 - Localizer reflection pattern

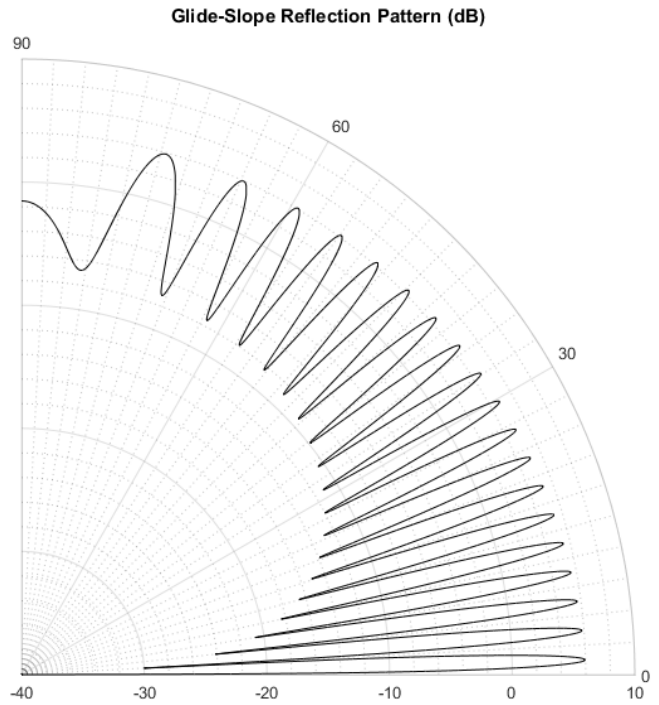

Figure 3.5.3 - Glideslope reflection pattern

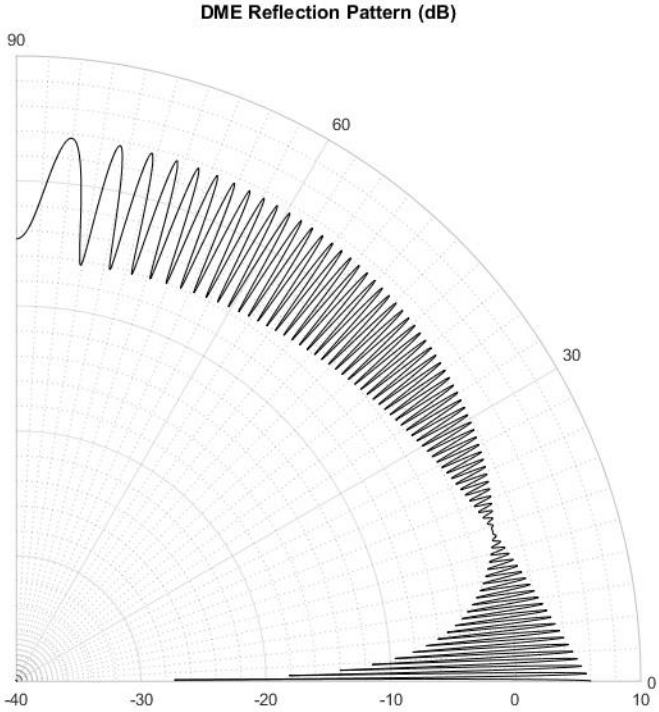

Figure 3.5.4 - DME reflection pattern

3.6 – ROUGHNESS AND REFLECTION SPREAD

Unless the reflection interface is perfectly flat, not all power within the reflected ray is directed at the receiver. A portion of the reflected power is scattered proportional to the degree of surface roughness. However, the portion of scattered power can be considered negligible if the reflection meets Rayleigh criterion. If this criterion is met, it can be approximated that total reflected power is directed at the receiver. Rayleigh criterion is described by [10]

$$\sigma_s < \frac{\lambda}{8\sin(\alpha)}. \tag{3.6.1}$$

The rms elevation, σ_s, is evaluated over a region under the propagation path containing all primary ground reflections. The point of reflection closest to the base station is 493 meters out and the furthest reflection is 1,550 meters out. The rms elevation was evaluated over the region 398 m < ρ < 1,697 m. This evaluation was performed by the math engine used to build this theoretical model, giving

$$\sigma_s = 1.58 \text{ m}.$$

To ensure the criterion is met for all values of α for all receiver heights, only the worst-case scenario of equation 3.6.1 needs to be evaluated. This would be at the highest receiver height, 1600 ft (488 m), for which α would be 0.0262 radians (1.5°). The derivation of this angle will be shown in the next section and accounts for refraction.

Checking each signal against the Rayleigh criterion produces the following results.

Signal	Rayleigh Criterion Met
Localizer	True
Glideslope	True
DME	False

Table 3.6.1 - Rayleigh Criterion

Because DME does not meet Rayleigh criterion, it cannot be approximated that the total reflected power is directed at the receiver. A roughness factor (RF) can be used to quantify this effect.

Roughness factor represents the portion of the reflected wave that is directed towards the receiver, with the remainder scattered. Roughness factor is described by [10]

$$RF(\alpha) = exp\left[-\frac{1}{2}\left(\frac{4\pi\sigma_s \sin(\alpha)}{\lambda}\right)^2\right]. \tag{3.6.2}$$

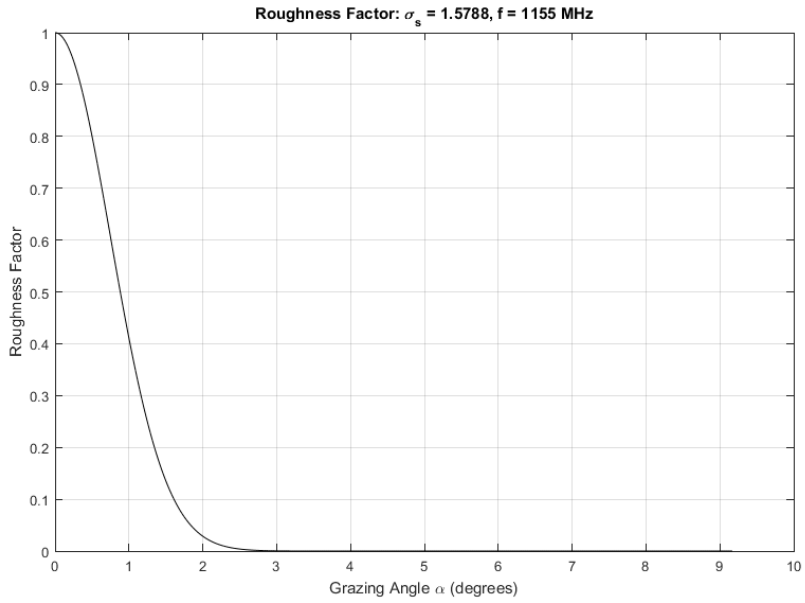

Figure 3.6.1 - DME roughness factor

Roughness factor applies to field strength and therefore should be inserted into the model as a multiplier of the reflected field's strength. It can be incorporated into a_2 of equation 3.5.1a for array factor.

The array factor weights for vertically polarized DME are

$$a_1 = 1 \text{ and } a_2 = -\Gamma(\alpha)RF(\alpha),$$

so, the array factor for DME is

$$Vertical\ Polarization\text{:}\ AF(\alpha) = 1 - \Gamma(\alpha)RF(\alpha)e^{\frac{j4\pi}{\lambda}h_{TX}\sin(\alpha)}. \tag{3.6.3}$$

Waves reflecting off a convex surface, like the Earth's curvature, spread out and lose power density. This loss in field strength of the reflected wave can be determined by divergence factor (DF) [11]

$$DF = \left[1 + \frac{2 * d_1 * d_2}{a * d * \tan(\alpha)}\right]^{-1/2}, \tag{3.6.4}$$

where d_1 and d_2 are the ground distances from the transmitter to the reflection point and from the reflection point to the receiver respectively. Calculated divergence factors for all receiver heights range from -0.16 to -0.02 dB. For most heights the associated losses are less than 0.1 dB, which is the level of precision of the measurement equipment. Because of this, the spread caused by reflection from a curved surface is negligible.

3.7 – WORKING INTO CARTESIAN COORDINATES

Thus far in chapter 3, refraction has remained mostly unincorporated in the model for EIRxP. For the polar reflection patterns to be transformed into cartesian coordinates, refraction should be incorporated. For a standard earth atmosphere, a ray propagated at $\alpha = 0°$ will pass below a receiver if the receiver has the same altitude as the transmitter. To hit a receiver at the same altitude as the transmitter, the ray must have a non-zero initial launch angle. The ray propagates with an initial launch angle and curves down while propagating to the receiver, forming an arc. The initial launch angle needed to reach a receiver with the same altitude of the transmitter can be found by [5]

$$\alpha_0 = \sqrt{h_m 2A'} \text{ radians}, \tag{3.7.1}$$

where h_m is the maximum bulge given by [5]

$$h_m = \frac{\left(\frac{d}{2}\right)^2}{2a}, \tag{3.7.2}$$

A' is a function of standard atmosphere refractivity gradient and Earth's radius given by [5]

$$A' = A - \frac{1}{6366\ \text{km}}, \tag{3.7.3}$$

and A is the refractivity gradient of a standard atmosphere given by [5]

$$A = 0.039 \times 10^{-6}.$$

The launch angle of the ray to the UAS based on receiver height can be approximated as

$$\alpha(h_{RX}) = \tan^{-1}\left(\frac{h_{RX}}{d}\right) + \alpha_0. \tag{3.7.4}$$

To perform a change of variables on the reflection patterns found in the previous section, the launch angles $\alpha(h_{RX})$ can be substituted in for α. This yields reflection pattern as a function of UAS altitude.

For localizer and glideslope,

$$RP(h_{RX})_{dB} = 20\log_{10}\left[1 + \Gamma\big(\alpha(h_{RX})\big)\exp\left[\frac{j4\pi}{\lambda}h_{TX}\sin\big(\alpha(h_{RX})\big)\right]\right]. \tag{3.7.5}$$

For DME,

$$RP(h_{RX})_{dB} = 20\log_{10}\left[1 - \Gamma\big(\alpha(h_{RX})\big)\mathrm{RF}\big(\alpha(h_{RX})\big)\exp\left[\frac{j4\pi}{\lambda}h_{TX}\sin\big(\alpha(h_{RX})\big) - \frac{1}{2}\left(\frac{4\pi\sigma_s\sin(\alpha)}{\lambda}\right)^2\right]\right]. \tag{3.7.6}$$

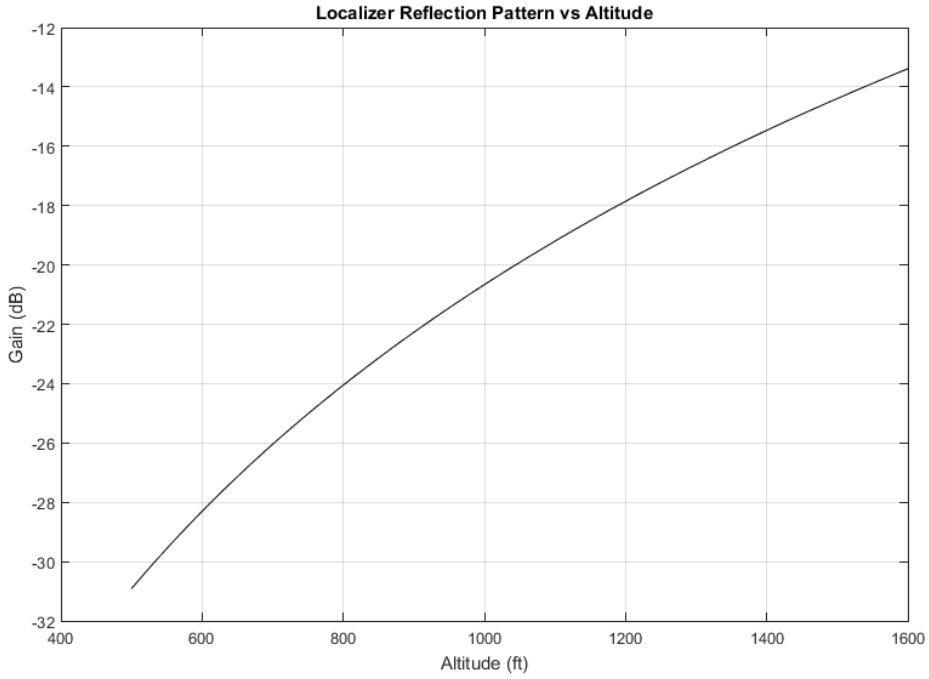

Figure 3.7.1 - Localizer reflection pattern vs altitude

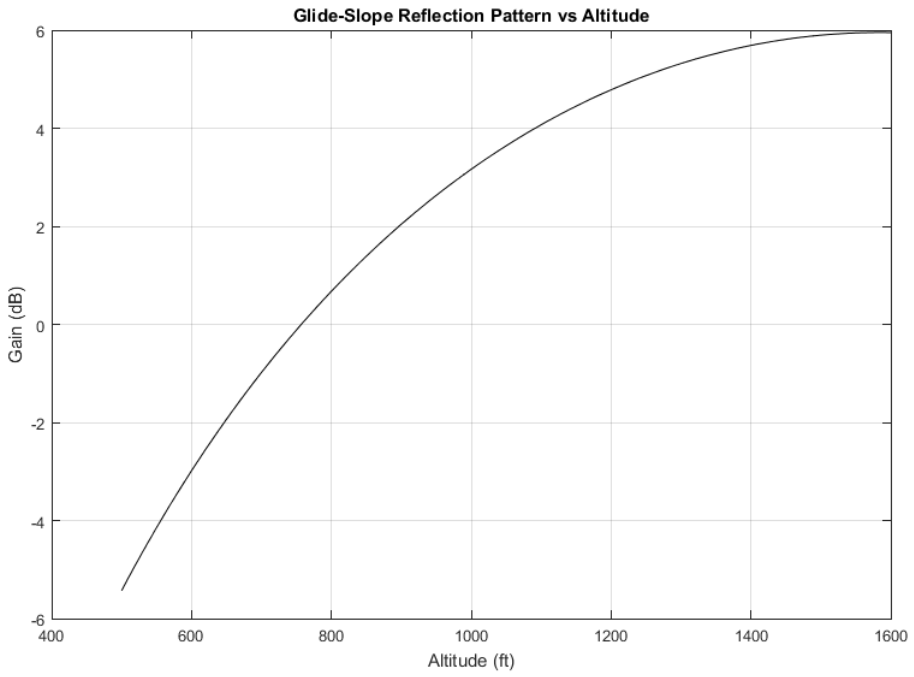

Figure 3.7.2 - Glideslope reflection pattern vs altitude

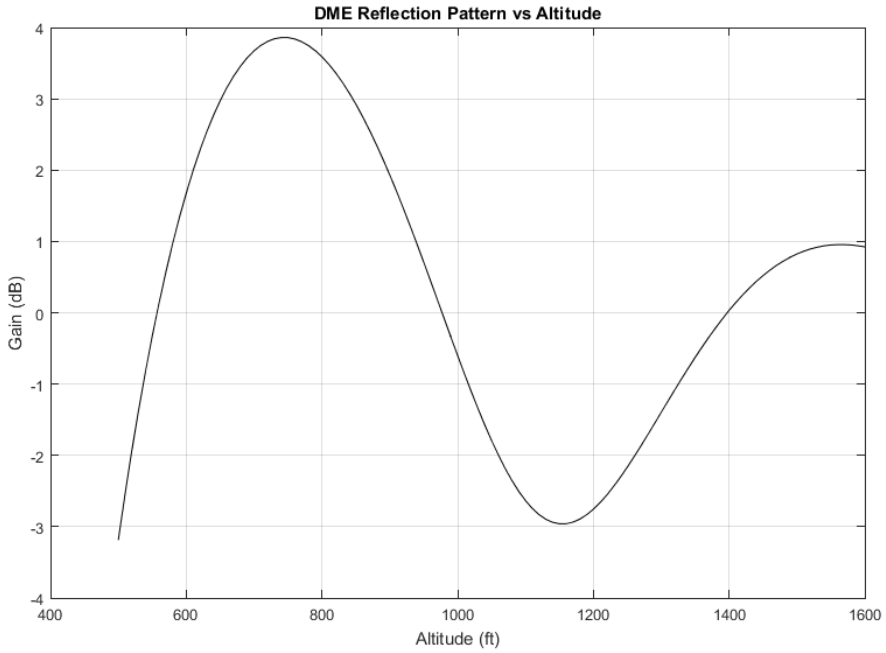

Figure 3.7.3 - DME reflection pattern vs altitude

The EIRxP can be found by using Frii's transmission equation with the derived reflection pattern incorporated:

$$EIRxP(h_{RX}) = P_{TX} + G_{TX} - PL_{dB} + RP(h_{RX})_{dB}. \quad (3.7.7)$$

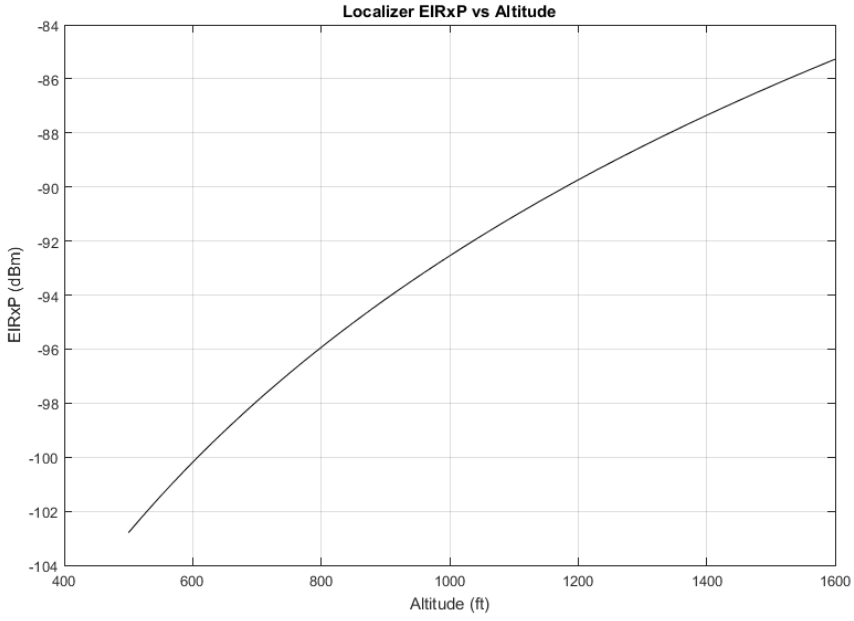

Figure 3.7.4 - Localizer EIRxP model

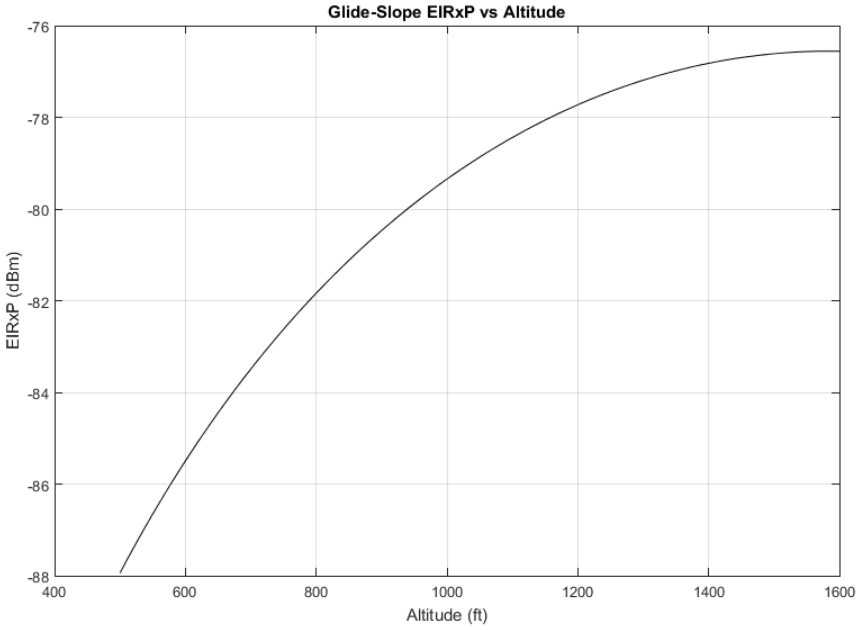

Figure 3.7.5 - Glideslope EIRxP model

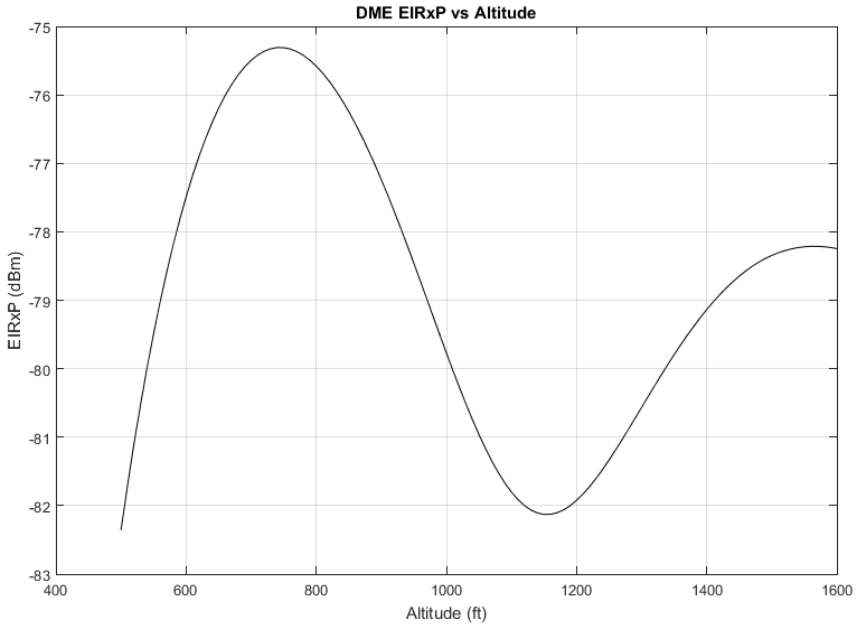

Figure 3.7.6 - DME EIRxP model

CHAPTER IV

EMPERICAL WORK

REFTAS, USRI, and the FAA teams worked together to acquire three sets of data during the year 2018. The first set was taken on June 6th and 14th, the second data set was taken on October 26th, and the last was taken on December 21st. A set consists of inspecting each of the ILS signals. For each signal three tests were performed. The three tests are vertical, isotropic, and horizontal sensitivity. The three tests for each of the three ILS signals makes nine total tests per data set. The tests are defined below.

Vertical Sensitivity - Channel power measurements are made at 100 ft (30.5 m) intervals between 500 ft (152 m) and 1400 ft (427 m) and at 10 ft (0.3 m) intervals between 1400 ft and 1600 ft (427 and 488 m) AGL. Measurements are made with the UAS's yaw oriented so that the receiver antenna's maximum directivity faces the transmitting base station. This test contains 30 measurements. The vertical sensitivity test is used to determine the effect of altitude on ILS signals.

Isotropic Sensitivity - Channel power measurements are made every 5 degrees through one full rotation. This measurement is taken at the airborne reference point at 1500 ft (457 m) AGL. The UAS starts the rotation facing north (0°) and progresses clockwise approaching an eastern heading first (90°). This test contains 72 measurements. The base station is located at 55° UAS heading, 10.5 nautical miles away.

Horizontal Sensitivity - Channel power measurements are made in a cross pattern at the reference altitude 1500 ft (457 m) AGL. One arm of the cross pattern moves the UAS axially in relation to the base station and the other arm follows angular movement. Measurements are indexed in order of measurement taken. Figures depicting the movement are in the next sections.

4.1 – DETERMINATION OF UAS RECEIVE ANTENNA GAINS

To find EIRxP, receiver gain (over isotropic) must be subtracted from the field measurements made in Tuttle. Receiver antenna gains were determined through tests conducted at the OSU Richmond Hill Research Complex. By measuring channel power of a radiated signal with frequency corresponding to that of the navigational aids, with the UAS-RX assembly and then with a reference antenna with known gain, receiver antenna gain can be found. This approach allows us to consider UAS structural EM effects. The third line on these tables describe the reference antenna's gains, which were determined experimentally. See figure 5.1 for an image of the UAS mounted in the anechoic chamber.

The DME monopole was damaged and subsequently rebuilt between the June and October flights. The gain calculated below is for post-rebuild. The gain before rebuilding was 1.4 dBi. The two different DME receive antenna gains were used accordingly throughout all calculations within this thesis.

$$G_{RX} = P_{RX} - P_{ref} + G_{ref} \tag{4.1.1}$$

DME Antenna Gain

Monopole Ch. Pow		-43.9 dBm
SAS-510-2 Ch. Pow	-	-37.2 dBm
SAS-510-2 Gain	+	7.0 dBi
Monopole Gain		0.3 dBi

Table 4.1.1 - DME antenna gain

Glideslope Antenna Gain

GS Dipole Ch. Pow		-30.5 dBm
SAS-510-2 Ch. Pow	-	-24.55 dBm
SAS-510-2 Gain	+	6.5 dBi
GS Dipole Gain		0.55 dBi

Table 4.1.2 - Glideslope antenna gain

Localizer Antenna Gain

LOC Dipole Ch. Pow		-25.1 dBm
SAS-517 Ch. Pow	-	-20.9 dBm
SAS-517 Gain	+	3.2 dBi
LOC Dipole Gain		-1.0 dBi

Table 4.1.3 - Localizer antenna gain

4.2 – JUNE DATA

In figure 4.2.2, localizer vertical sensitivity measurements show a rise in power over elevation. The measurements taken between 1400 and 1600 ft (427 and 488 m) show small incremental changes, except for the 0.4 dBm jump from 1540 to 1550 ft (469 to 472 m). A characteristic dipole pattern can be seen in localizer isotropic sensitivity (figure 4.2.3). In all isotropic sensitivity measurements using a dipole receiver, the antenna is mounted at a 90° on the aircraft. This displaces the heading that the boresight of the antenna would be pointed towards the base station from 55° to -35° or 355°. The arrow on the figure represents the region in the pattern that faces the base station. Localizer horizontal sensitivity has a 0.2 dB spread (figure 4.2.4). After June the reference point was moved slightly to not be over the high school. Compare figures 4.2.1 and 4.3.1.

Figure 4.2.5 shows the glideslope vertical sensitivity measurements. They increase to a maximum channel power at around 1400 ft (427 m) after which the channel power curves off forming an arcing pattern. The arc is mostly smooth but contains a 0.7 dBm decrease from 1500 to 1540 ft (457 to 469 m). Glideslope isotropic sensitivity also bears its dipole pattern. The gap from 355° to 0° when the aircraft returns to its initial heading is 2.3 dBm. Glideslope horizontal sensitivity has a spread of 1.6 dBm. It seems to have 3 distinct sections that the data groups into. The speculation was that the sections correlated to the arm section of the cross pattern that the UAS flies. This is the reason for changing the order that the measurement points are taken in. Compare figures 4.2.1 and 4.3.1.

DME vertical sensitivity has a local maximum at 750 ft (229 m) and a diminished region at 1100 ft (335 m). This is due to the interference between line-of-sight and reflected rays as seen in the previously covered EIRxP model. Between 1400 ft and 1600 ft (427 and 488 m) the channel power rises steadily. DME isotropic sensitivity measurements are consistent between 45° and 70°. Within these headings channel power measurements change no more than 0.1 dBm from the

base station heading of 55°. The fluctuations that occur outside of these headings are likely due to interference from the UAS structure. DME horizontal sensitivity measurements have a spread of 2.1 dBm. This horizontal sensitivity pattern seems more sporadic than the previous two.

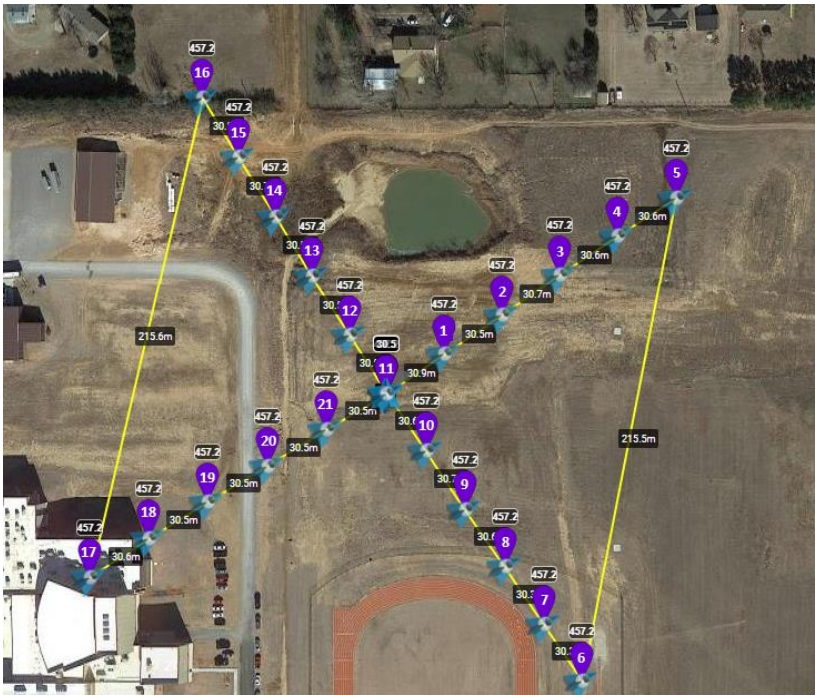

Figure 4.2.1 - June horizontal sensitivity flight pattern

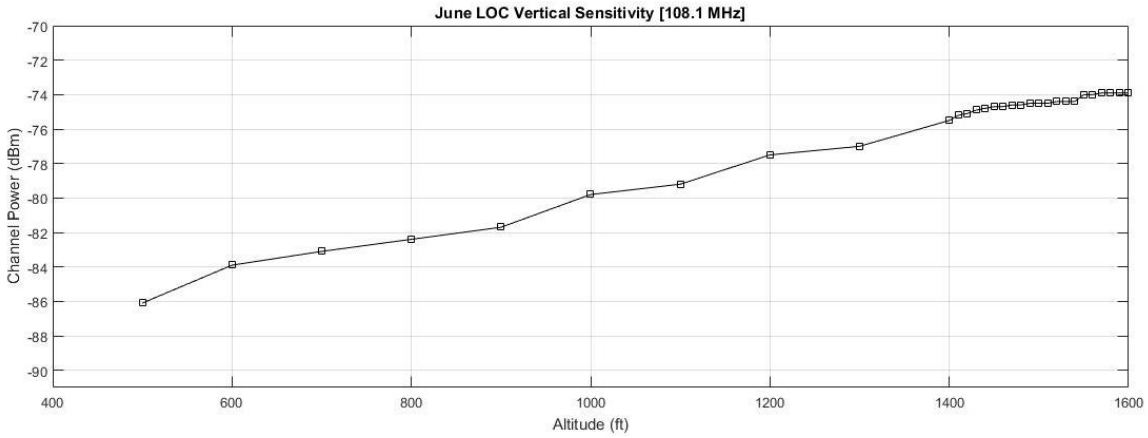

Figure 4.2.2 - June localizer vertical sensitivity

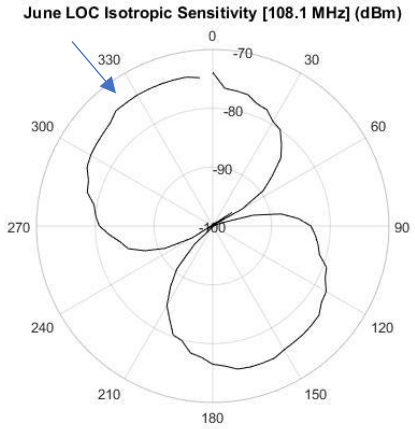

Figure 4.2.3 - June localizer isotropic sensitivity (arrow indicates antenna boresight)

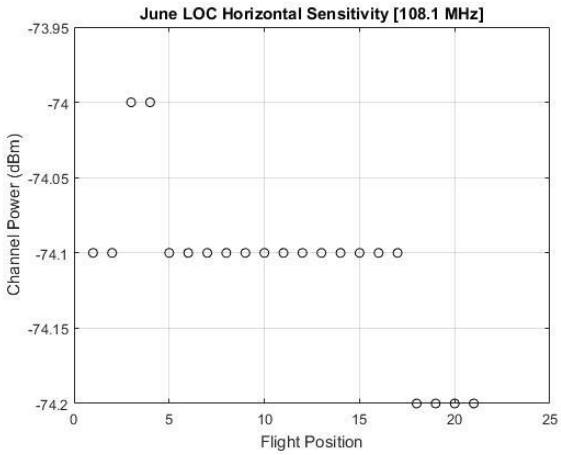

Figure 4.2.4 - June localizer horizontal sensitivity

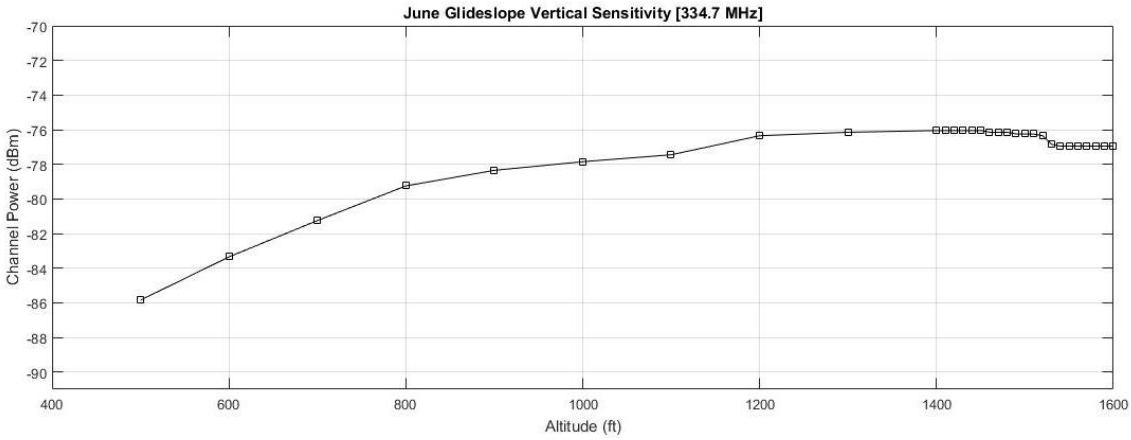

Figure 4.2.5 - June glideslope vertical sensitivity

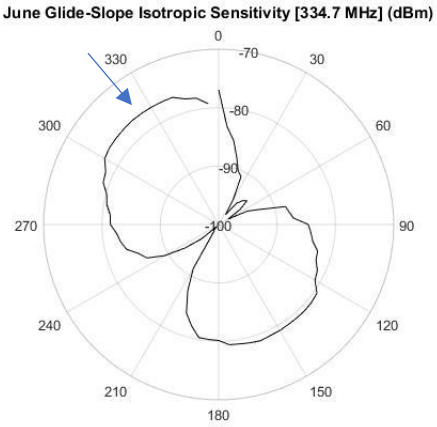

Figure 4.2.6 - June glideslope isotropic sensitivity (arrow indicates antenna boresight)

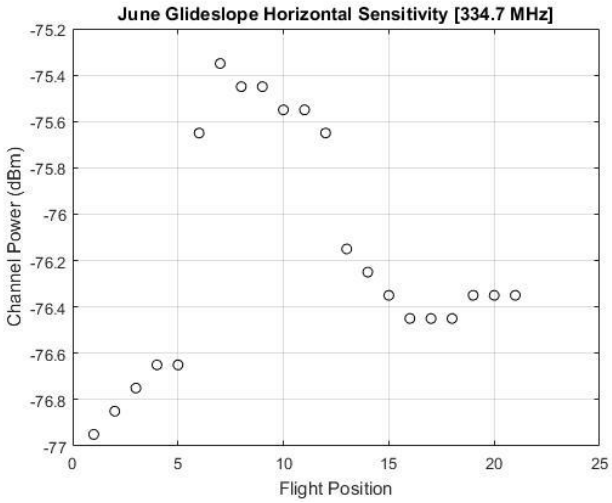

Figure 4.2.7 - June glideslope horizontal sensitivity

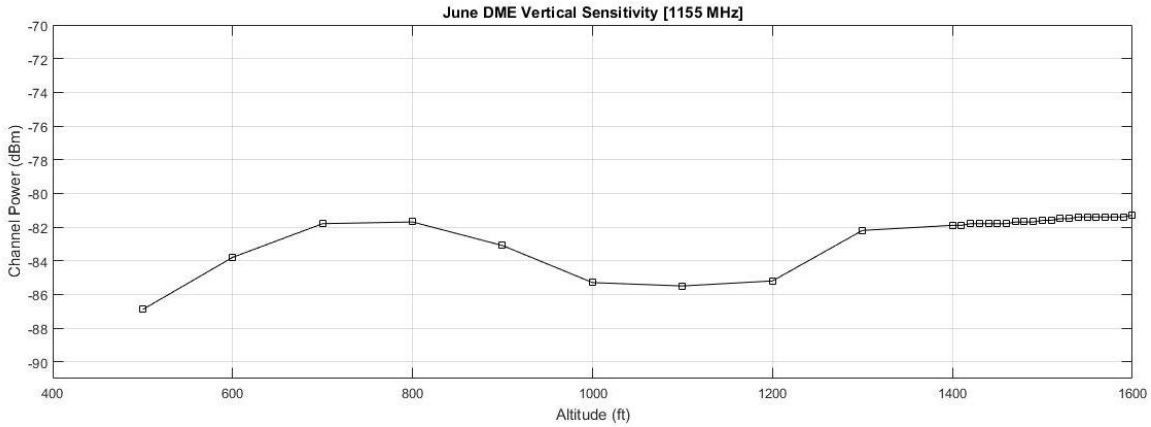

Figure 4.2.8 - June DME vertical sensitivity

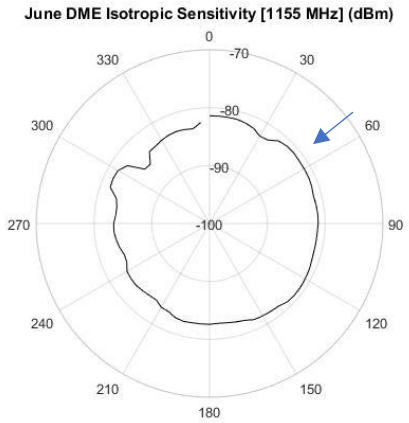

Figure 4.2.9 - June DME isotropic sensitivity (arrow indicates antenna boresight)

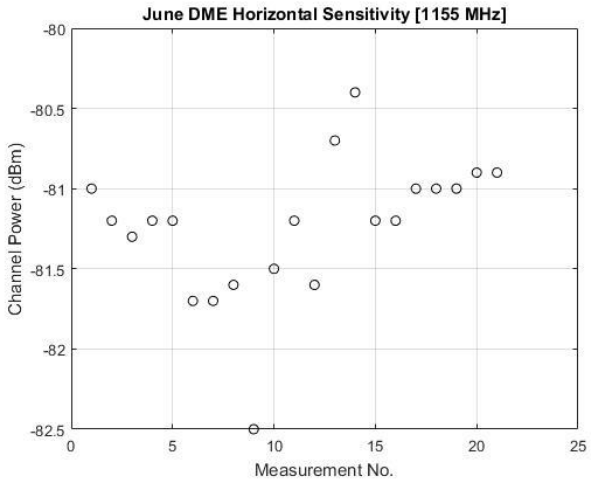

Figure 4.2.10 - June DME horizontal sensitivity

4.3 – OCTOBER DATA

Localizer vertical sensitivity measurements rise as we would expect based on June data up to 1400 ft (427 m). The jump at 1400 ft is 1.2 dBm and the jump at 1560 ft (475 m) is 0.4 dBm. The localizer isotropic sensitivity shows a dipole as it did in June but with a smaller bump in measured power when returning to initial heading. Localizer horizontal sensitivity spread is 0.4 dBm. The measurement for 1420 ft (443 m) is missing. This is either due to the UAS controller failing to send the trigger signal or the spectrum analyzer failing to detect the trigger signal.

Glideslope vertical sensitivity has a maximum at 1460 ft (445 m). Between 1500 and 1600 ft (457 and 488 m) the channel power decreases less dramatically than previously. Instead of a jump in channel power this flight captured a more stable decrease above 1500 ft (457 m). A dipole pattern is visible in the glide-slope isotropic sensitivity. The jump from 355° and 0° is 2.3 dBm. Continuity from 355° and 0° is better than in the June flight. Glideslope horizontal sensitivity has a spread of 1.1 dBm. Variance is higher in the angular direction ("side-to-side") than in the radial direction (distance from transmitter).

DME vertical sensitivity is like that of June. For this flight the area beyond the second constructive lobe is showing above 1500 ft (457 m). DME isotropic sensitivity has a similar pattern to that of June. DME horizontal sensitivity measurements have a channel power spread of 1.8 dB, compared to 2.1 dBm previously. As with glide-slope, variance is higher in the angular direction ("side-to-side") than in the radial direction (distance from transmitter). The large spreads in glideslope and DME horizontal sensitivity could be caused by the UAS not fully stabilizing while taking the individual measurements. The time the UAS stabilized at each position was at this point changed from 1 to 3 seconds.

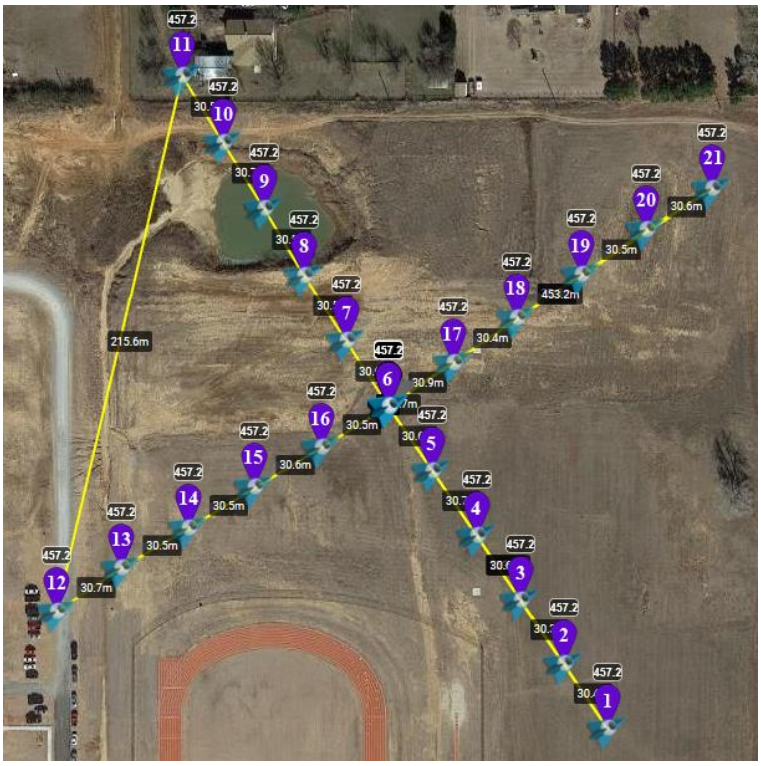

Figure 4.3.1 - October and December horizontal sensitivity flight pattern

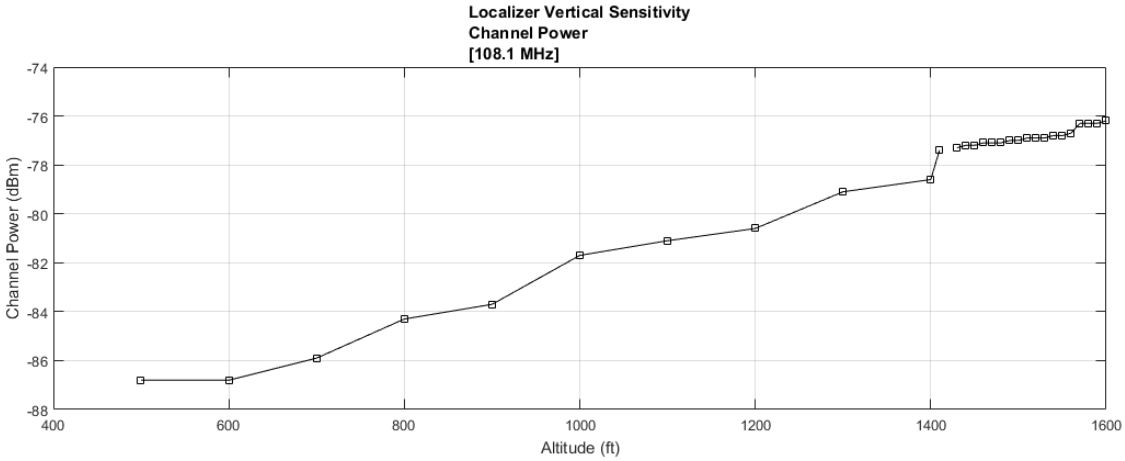

Figure 4.3.2 - October localizer vertical sensitivity

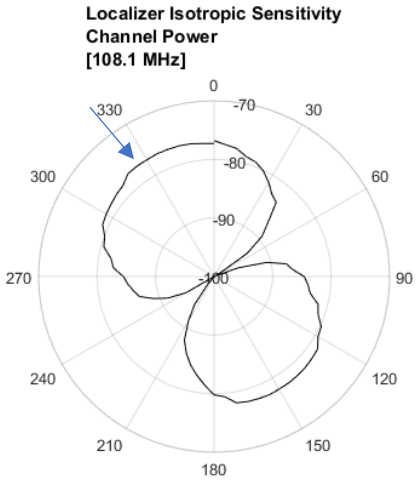

Figure 4.3.3 - October localizer isotropic sensitivity (arrow indicates antenna boresight)

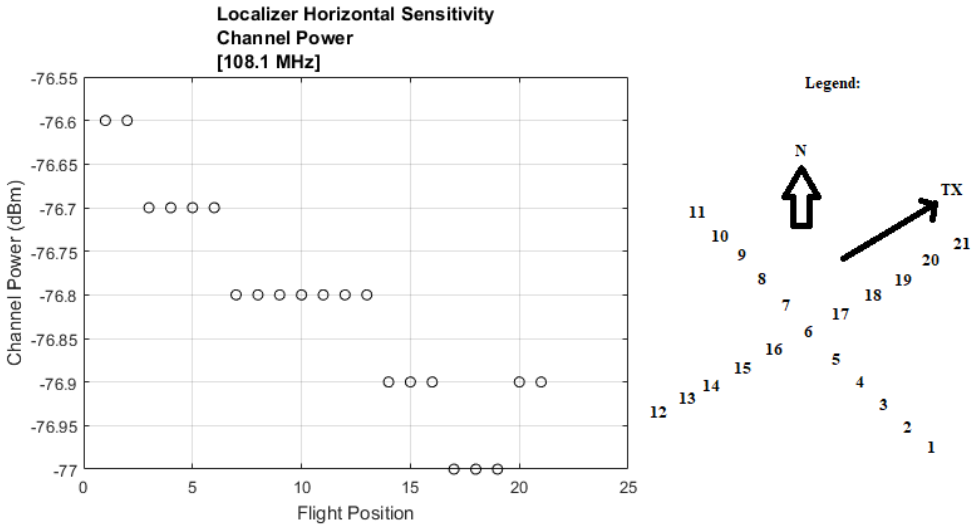

Figure 4.3.4 - October localizer horizontal sensitivity

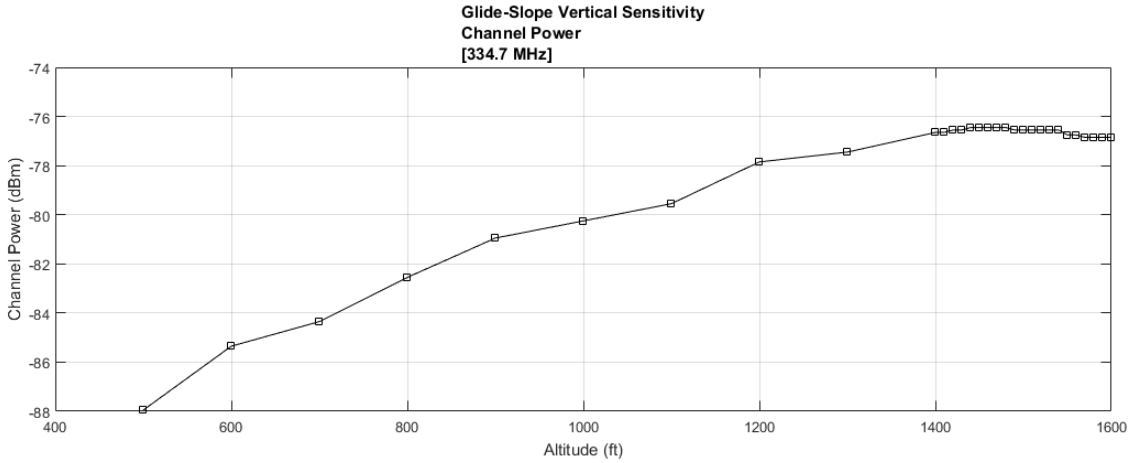

Figure 4.3.5 - October glideslope vertical sensitivity

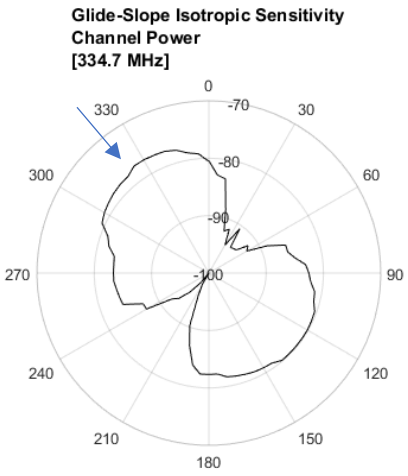

Figure 4.3.6 - October glideslope isotropic sensitivity (arrow indicates antenna boresight)

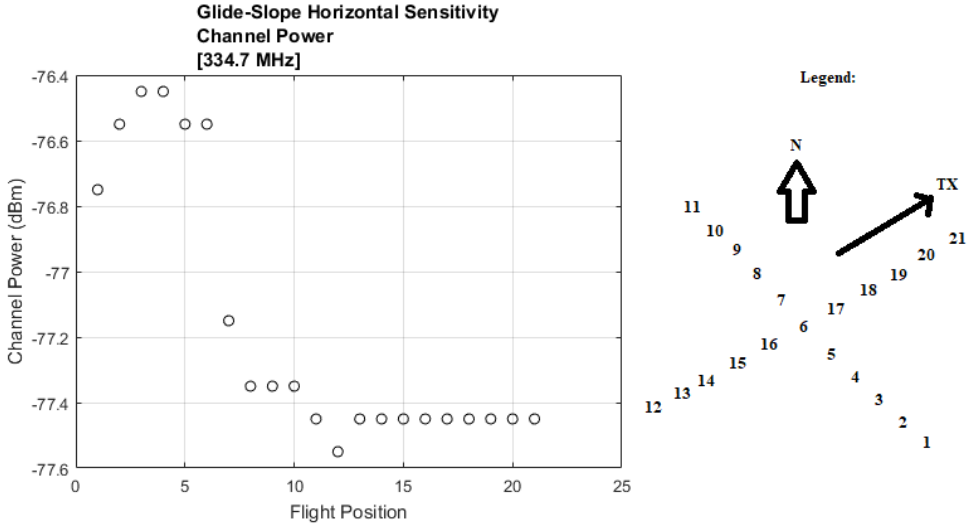

Figure 4.3.7 - October glideslope horizontal sensitivity

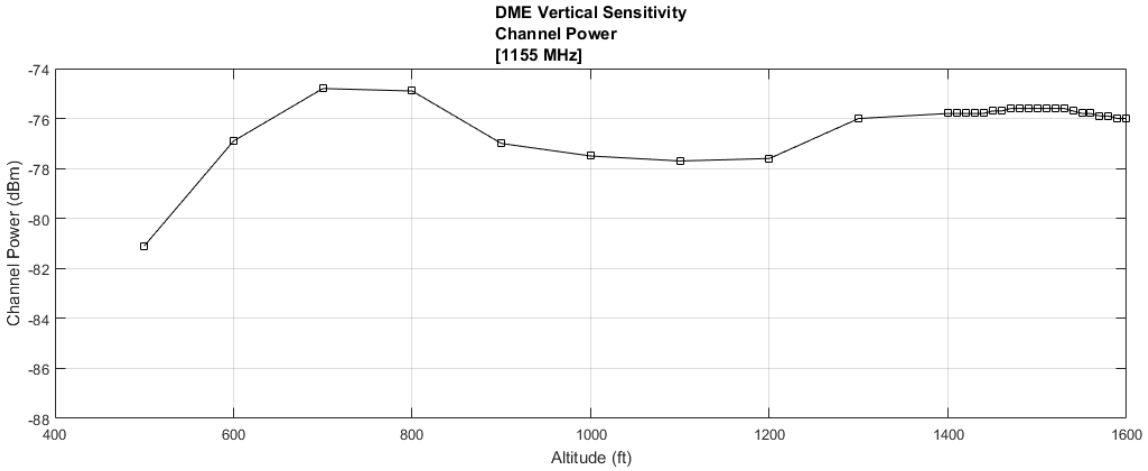

Figure 4.3.8 - October DME vertical horizontal sensitivity

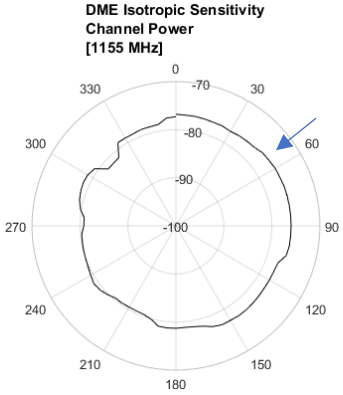

Figure 4.3.9 - October DME isotropic sensitivity (arrow indicates antenna boresight)

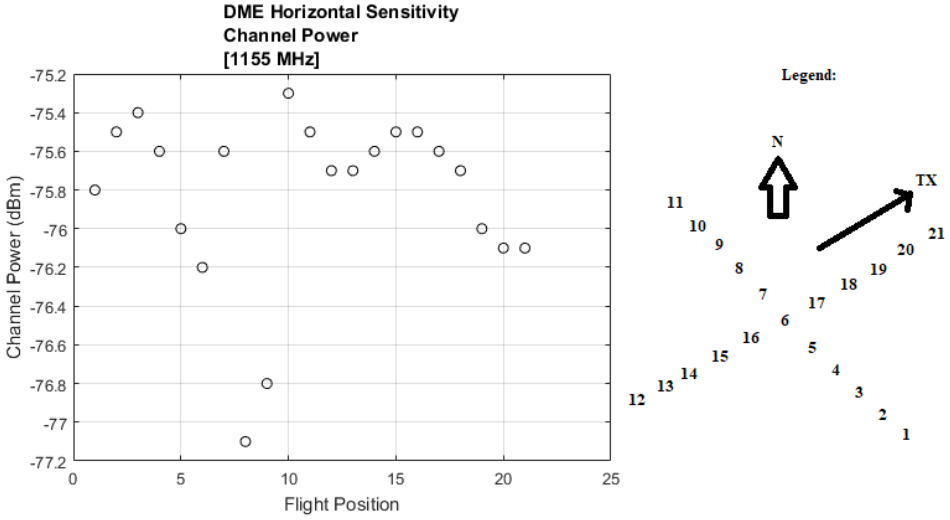

Figure 4.3.10 - October DME horizontal sensitivity

4.4 – DECEMBER DATA

Before the December campaign the stabilization of the UAS was increased from 1 to 3 seconds. The results of the tests taken in December closely resemble those of October. Localizer vertical sensitivity has a gap at 1400 ft (427 m) like October's data. This gap is 1.0 dB. Localizer horizontal sensitivity has a spread of 0.2 dBm like in June, back down from 0.4 dB in October.

Glideslope vertical sensitivity has a maximum at 1530 ft (466 m). As in October the back side of the lobe is visible at high altitude. Because of the increase in stabilization time, glideslope horizontal sensitivity spread is down to 0.5 dBm. Previously this spread was 1.1 and 1.6 dBm.

DME vertical sensitivity has a local maximum at 800 ft (244 m) and a diminished region at 1300 ft (396 m). The measurements above 1400 ft (427 m) are not as smooth as they have previously been. DME horizontal sensitivity measurements have a spread of 2.0 dBm. This is like June and October figures. The lengthened stabilization period did not seem to help at DME frequencies.

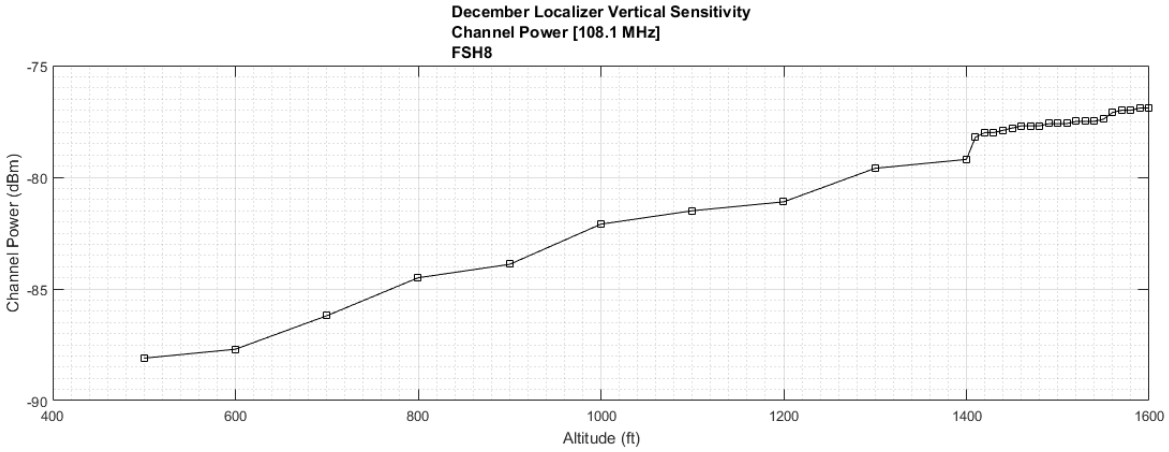

Figure 4.4.1 - December localizer vertical sensitivity

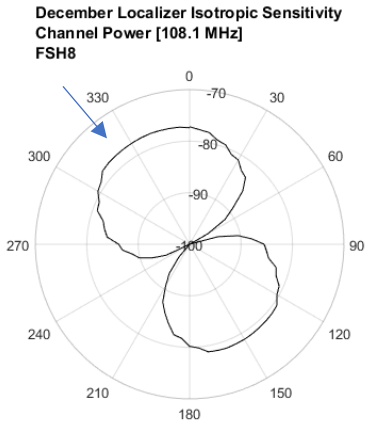

Figure 4.4.2 - December localizer isotropic sensitivity (arrow indicates antenna boresight)

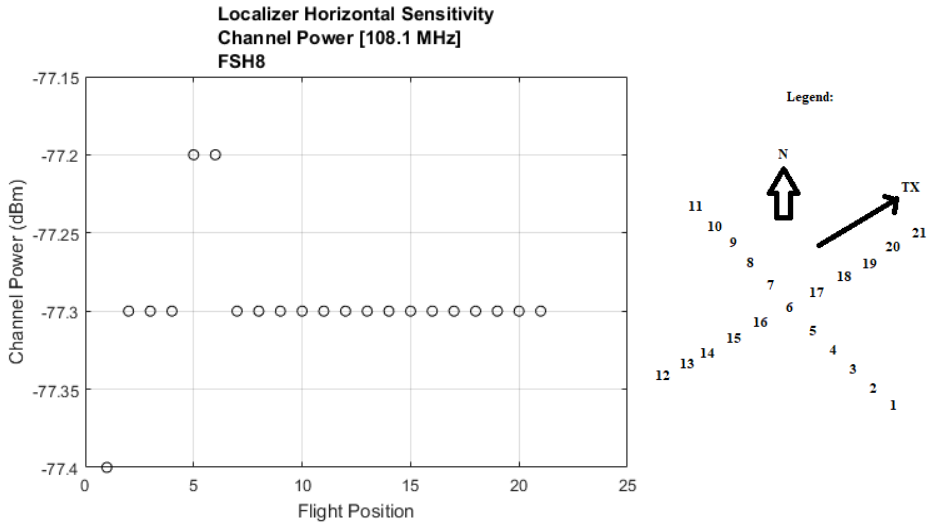

Figure 4.4.3 - December localizer horizontal sensitivity

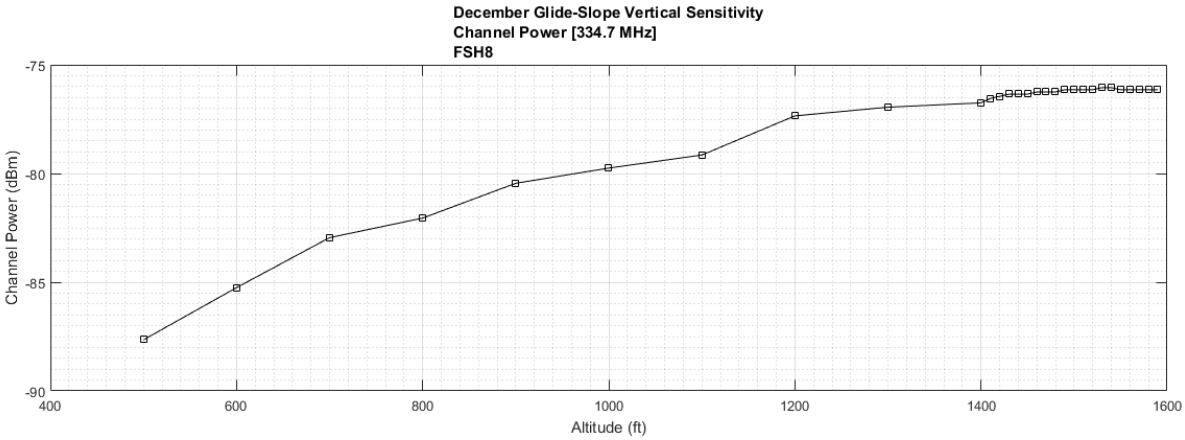

Figure 4.4.4 – December glideslope vertical sensitivity

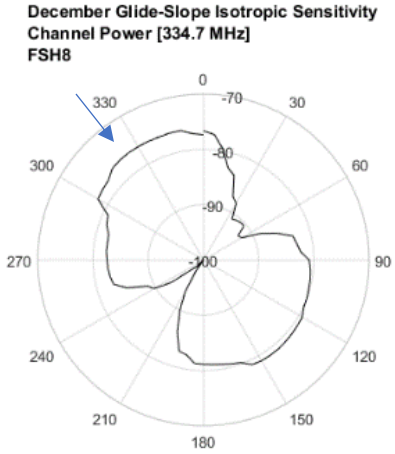

Figure 4.4.5 - December glideslope isotropic sensitivity (arrow indicates antenna boresight)

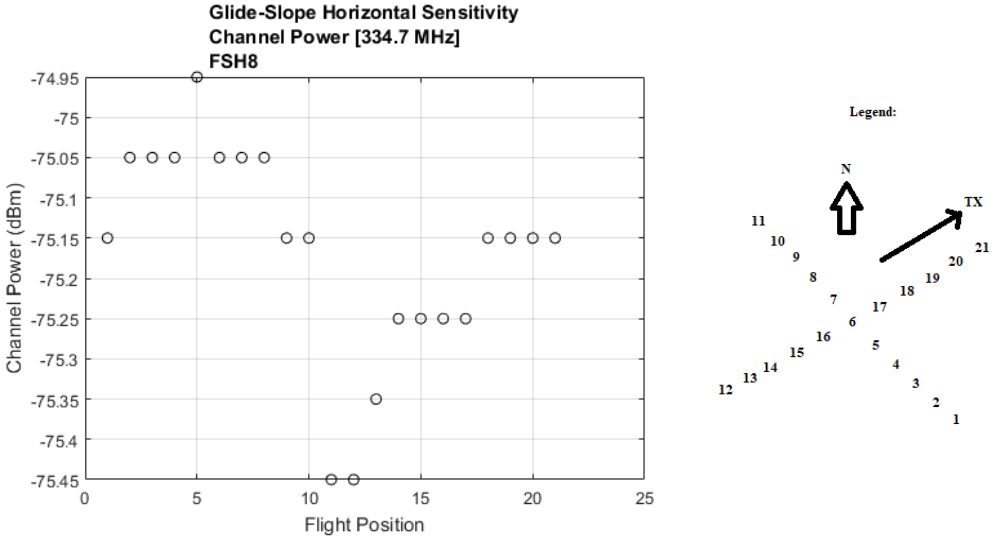

Figure 4.4.6 - December glideslope horizontal sensitivity

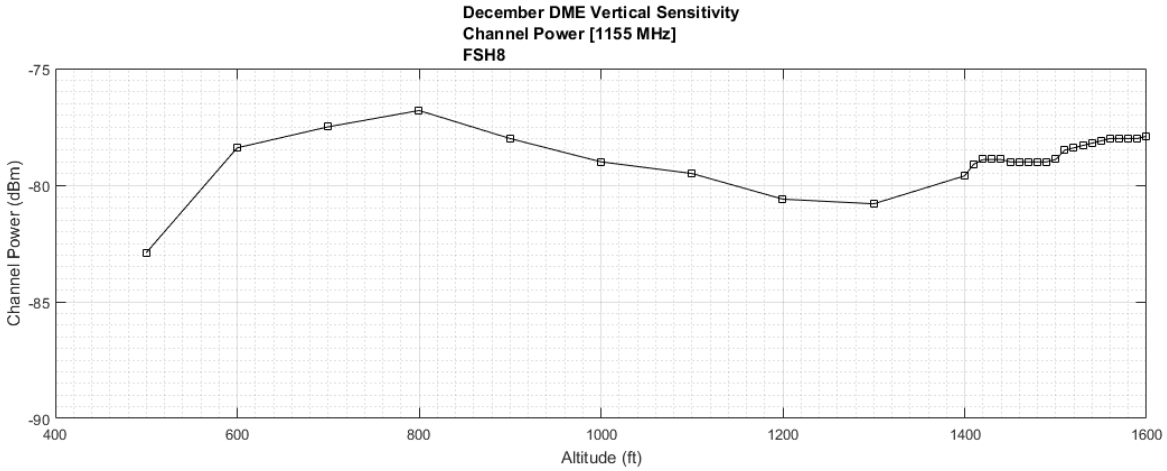

Figure 4.4.7 - December DME vertical sensitivity

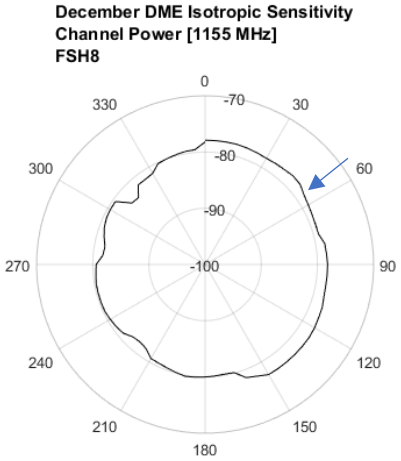

Figure 4.4.8 - December DME isotropic sensitivity (arrow indicates antenna boresight)

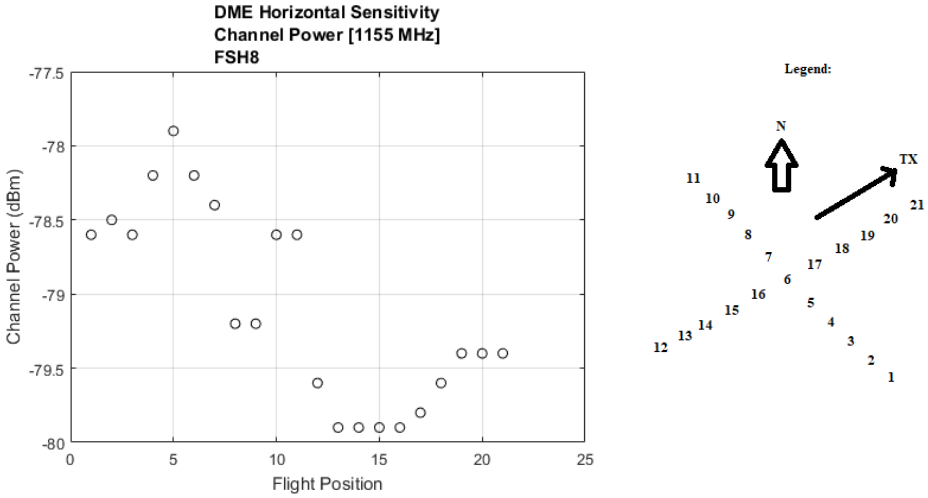

Figure 4.4.9 - December DME horizontal sensitivity

4.5 – COMBINED TEST DATA

Plotting the test data together clearly shows the change in measurements between test dates. June localizer data seemed to be higher all around while October and December localizer data were very similar. The month-to-month differences in channel power is likely attributed to changing atmospheric conditions or small changes in transmitter orientation at the base station upon reassembly. Most differences are less than 3 dB apart, the exception being between June and October DME measurements. A commonly used parameter in antenna theory is half-power beam width, which could be considered the working region of an antenna. So, by that metric, these measurements are reasonably repeatable.

	Reference Point Measurements								
	June			October			December		
Signal	V	H	I	V	H	I	V	H	I
Localizer	-74.5	-74.1	-74.4	-77	-76.7	-77	-77.6	-77.2	-77.5
Glideslope	-76.2	-76.6	-76.8	-76.5	-76.5	-77.2	-76.1	-75	-76.3
DME	-81.6	-81.7	-81.1	-75.6	-76.2	-76.3	-79.1	-78.2	-78.5

Table 4.5.1 - Reference point measurements [V: vertical sensitivity, H:horizontal sensitivity,I: isotropic sensitivity]

For all three months the measured localizer channel power rises with altitude. This happens because of the lobing of the reflection pattern. The UAS never reaches the peak of the first lobe. Localizer has such tall lobes because of the large wavelength it has relative to transmitter height.

June data contained the highest power for glideslope vertical sensitivity, but June data was not the highest for isotropic and horizontal sensitivity. Here the UAS reaches the first lobe and partially passed above it. The UAS manages to reach past the first lobe because the glideslope lobing pattern is more compact than localizer. The wavelength-to-transmitter-height ratio is higher here than in localizer.

The measured channel power changed a couple dB between June, October, and December for DME. In each DME test June had the lowest measurements, October had the highest measurements, and December floats in between. This trend is true for almost all DME data points. The exception is in DME isotropic sensitivity. December data gets as high as October data

in some regions. The UAS reaches through the first lobe, through the null, and into the second lobe. The ratio of wavelength to transmitter height is higher here than in localizer and glideslope. This allows the UAS to move through more lobes because they are relatively short.

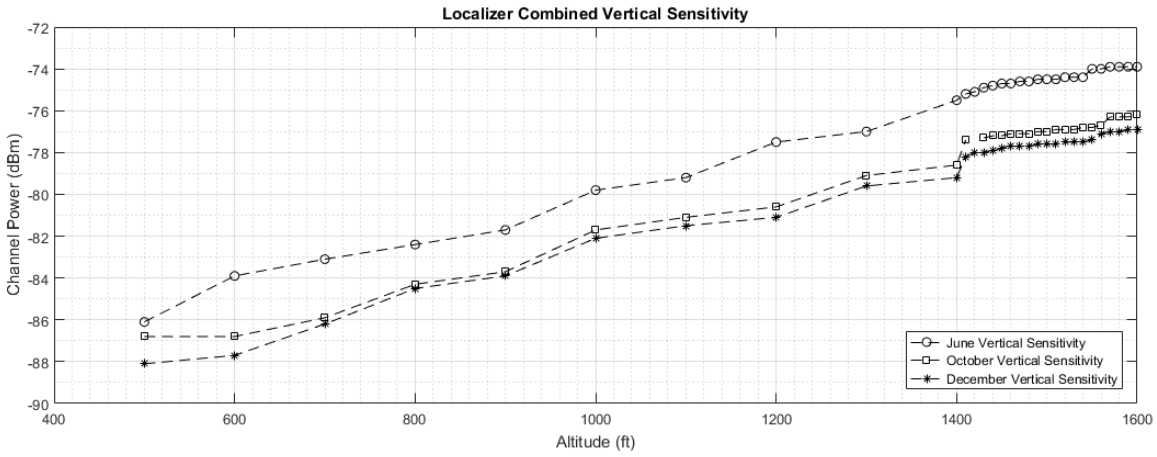

Figure 4.5.1 - Combined localizer vertical sensitivity

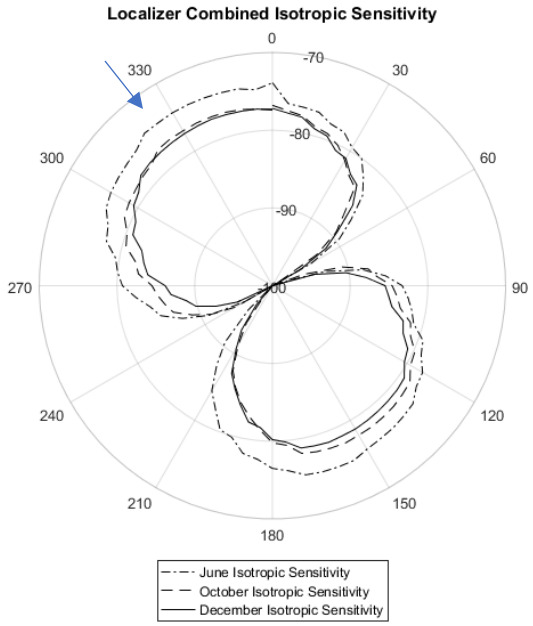

Figure 4.5.2 - Combined localizer isotropic sensitivity (arrow indicates antenna boresight)

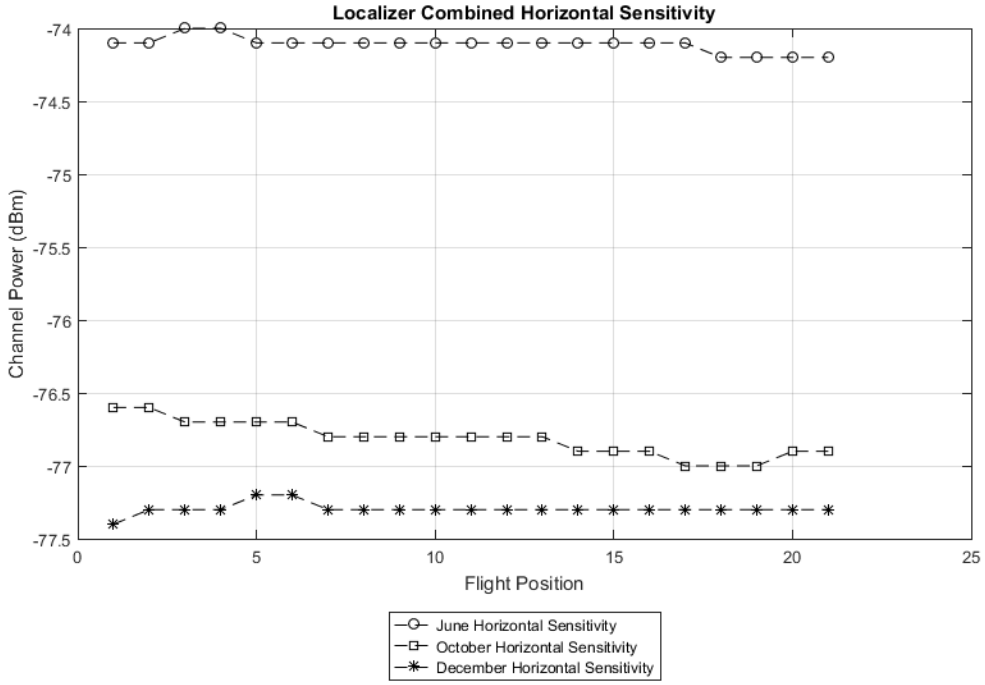

Figure 4.5.3 - Combined localizer horizontal sensitivity

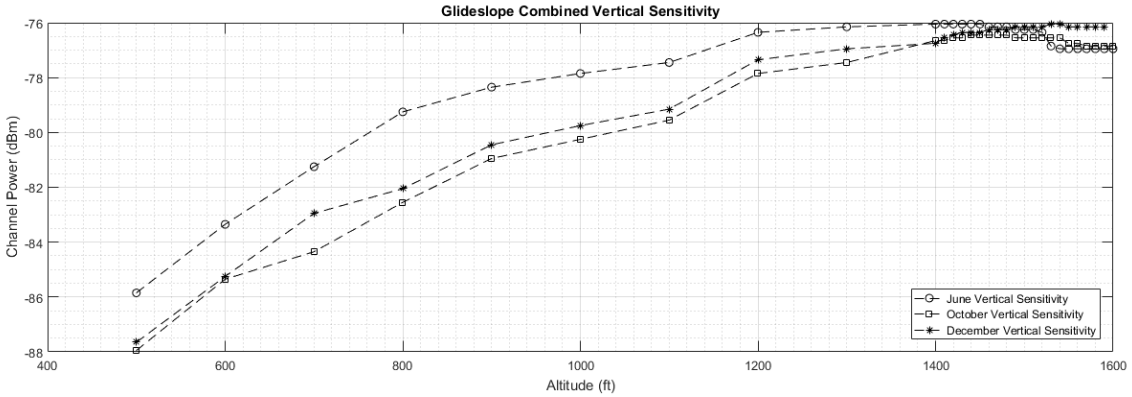

Figure 4.5.4 - Combined glideslope vertical sensitivity

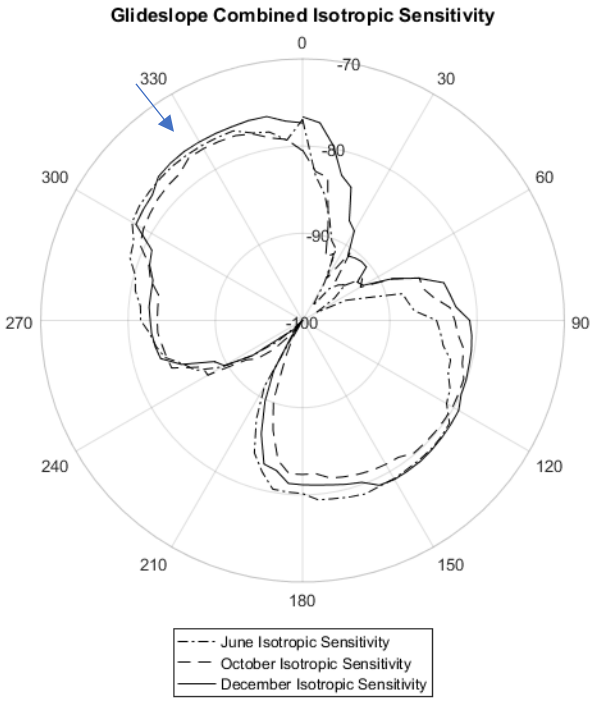

Figure 4.5.5 - Combined glideslope isotropic sensitivity (arrow indicates antenna boresight)

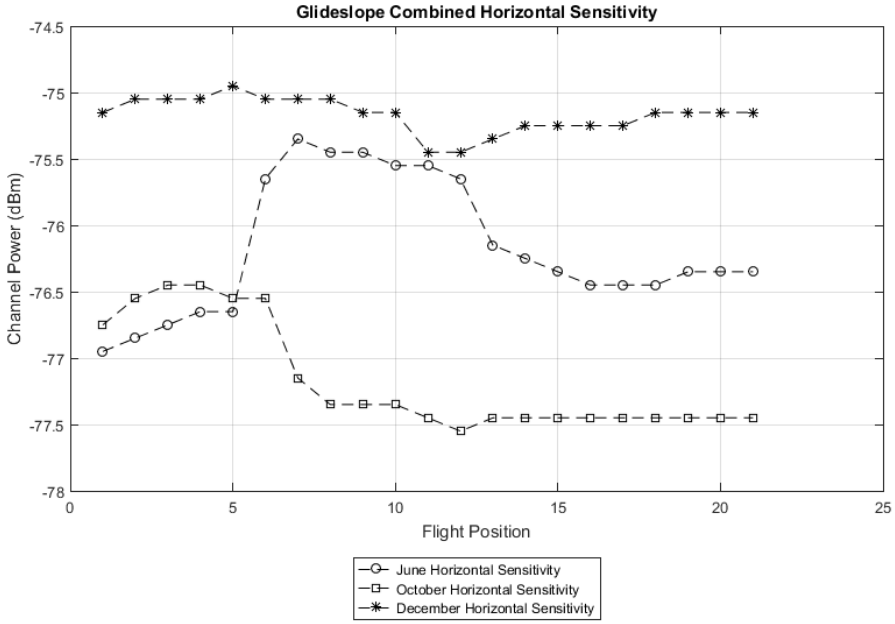

Figure 4.5.6 - Combined glideslope horizontal sensitivity

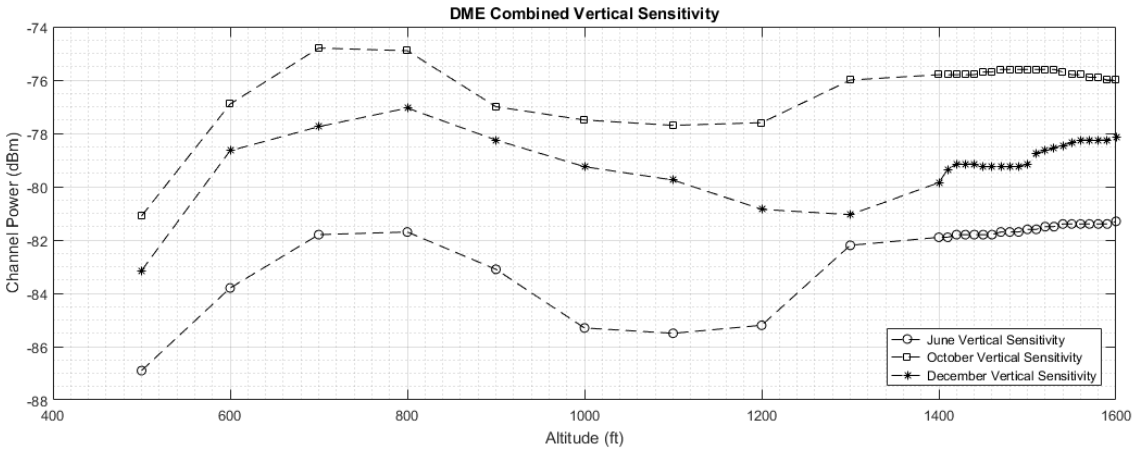

Figure 4.5.7 - Combined DME vertical sensitivity

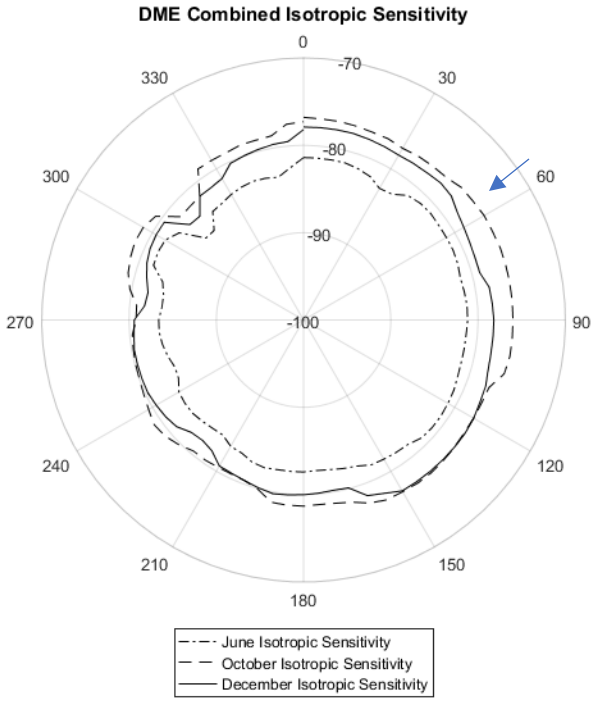

Figure 4.5.8 - Combined DME isotropic sensitivity (arrow indicates antenna boresight)

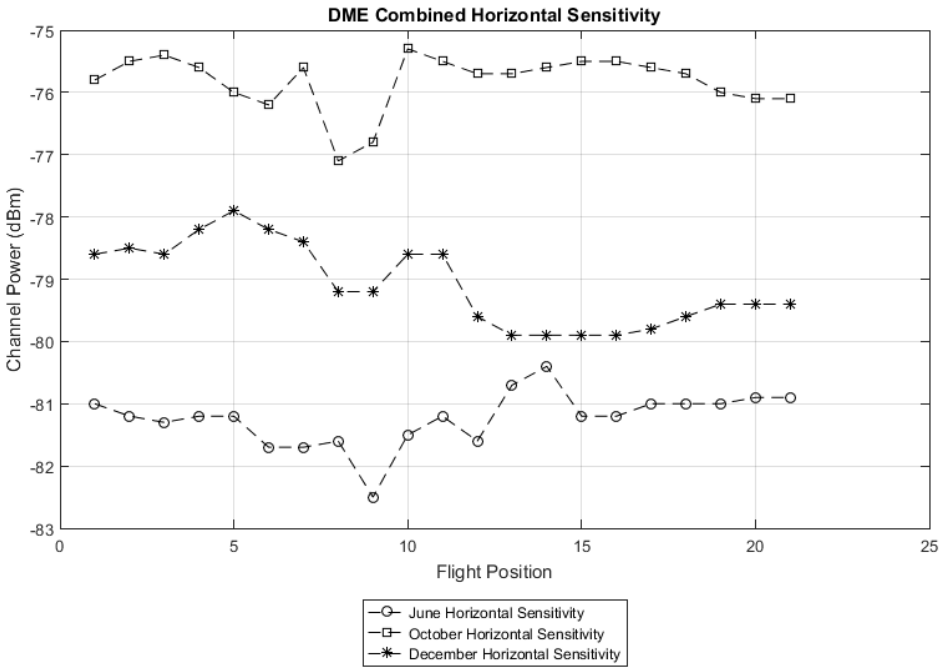

Figure 4.5.9 - Combined DME horizontal sensitvity

4.6 – COMPARISON TO MODEL

The localizer model increases with altitude without reaching the peak of the first lobe, just as the empirical data. The is a difference between the model and empirical data of approximately 10-15 dB. This is likely due to losses incurred by not sufficiently exiting the half-wave ground Fresnel zone. Even without direct ground obstruction, there can exist significant transmission losses due to diffraction effects [11]. Figure 4.6.2 shows the extent to which the localizer line-of-sight ray is within the half-wave ground Fresnel zone at 1500 ft (457 m). The line-of-sight path passes through more of the half-wave ground Fresnel zone at lower altitudes.

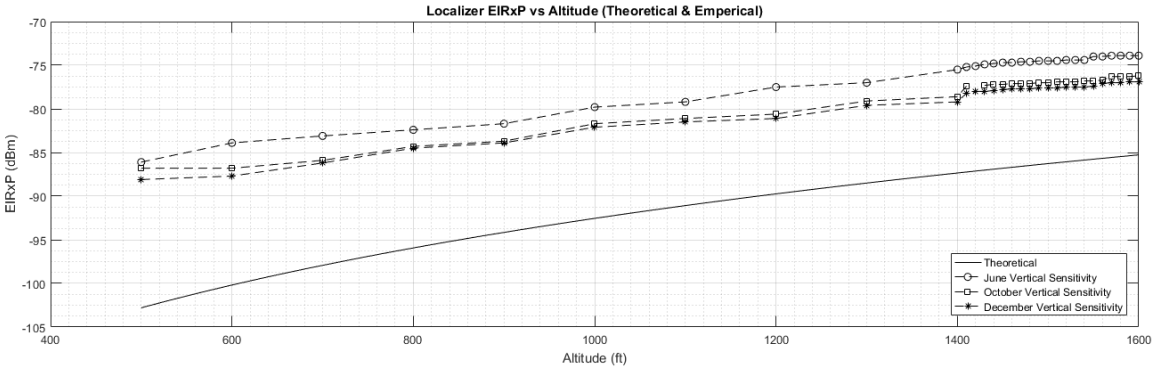

Figure 4.6.1 - Localizer theoretical model vs empirical data

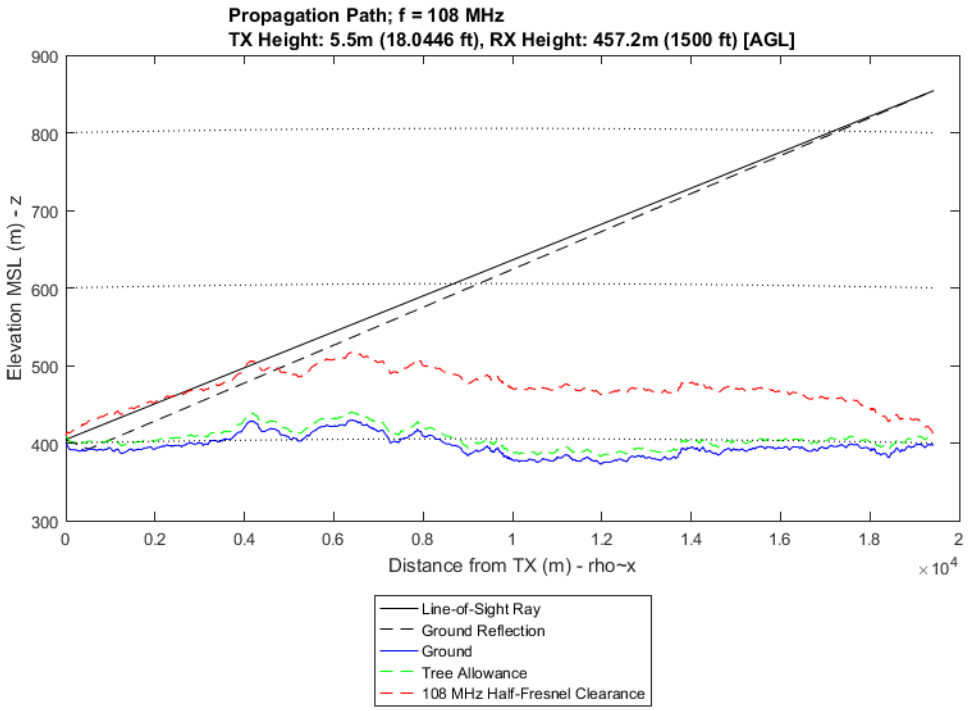

Figure 4.6.2 - Localizer propagation path

The glideslope model fits well between the empirical data. The model does not pass over the first lobe as the empirical data does, but it comes close. The model level closely matches the October and December data, with the June data hovering 2 dB over for most altitudes.

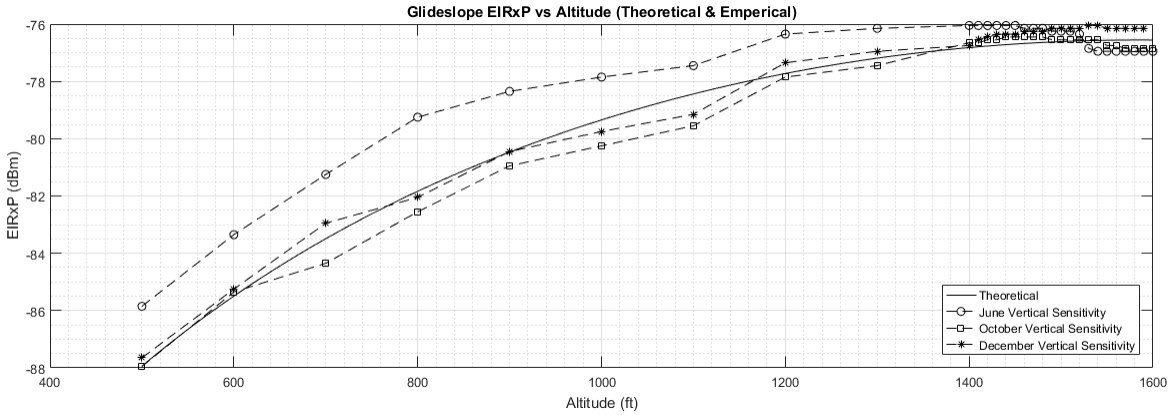

Figure 4.6.3 - Glideslope theoretical model vs empirical data

The DME model is saddled between the empirical data. October empirical data is higher than the model, June empirical data is lower, and December empirical data is the closest, level-wise, to the model. The variance in empirical data is likely due to the sensitivity of the relatively small-wavelength DME to changes in transmitter height, placement, and orientation as well as atmospheric conditions. The model accurately predicts the first lobe for all empirical data at approximately 750 ft (229m). The model's first null altitude nearly matches June and October data at approximately 1150 ft (350 m). December's data has its null at approximately 1300 ft (396 m).

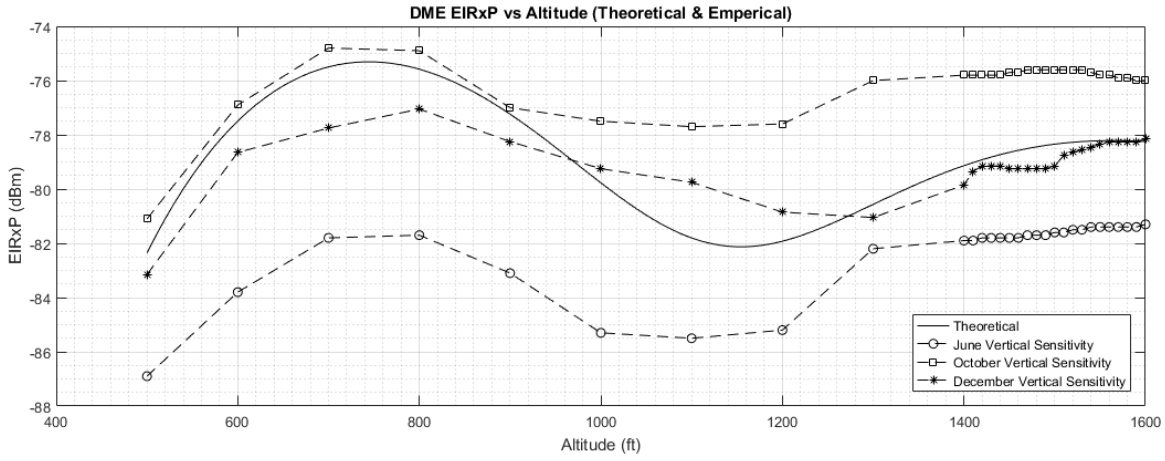

Figure 4.6.4 - DME theoretical model vs empirical data

CHAPTER V

CHANNEL POWER CORRECTION BASED ON UAS ORIENTATION

In an ideal scenario the UAS is perfectly stable and orienting the antenna into the correct heading. In a realistic scenario this is nearly impossible. A potentially useful feature to this system would be a correction to the measured channel power dependent upon UAS orientation at the time of capture. Because the receiver antenna is not isotropic and because the carbon fiber UAS frame can interfere with incident waves, measured channel power will vary with vehicle pitch, roll, and yaw.

The method for correcting this error is as follows.

1. Place the UAS with antenna in an anechoic chamber.
2. Take channel power measurements over different pitch-yaw positions with constant transmitter power.
3. Create a gradient with the data.
4. Inversely apply the data gradient to field data for correction.

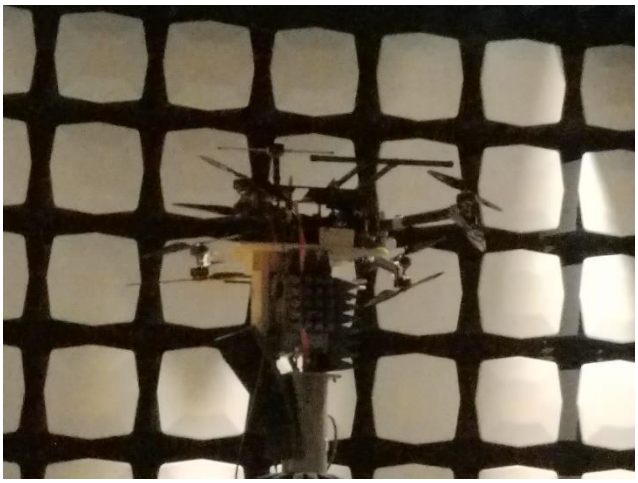

Figure 5.1 - UAS in anechoic chamber

The table below contains raw channel power measurements from the anechoic chamber. The measurements were taken at 5° increments. This data was then normalized to boresight. The normalized data is in reference to the measurement taken at 0° pitch and 0° yaw. This was then interpolated to produce a finer gradient (figure 5.2). In general, it is visible that when pitching up the antenna acquires a gain and acquires losses when pitching down. This is due to the landing gear moving into the field of view of the antenna while pitching down. The variations in yaw are likely due to the glideslope dipole receiver being improperly balanced and being mounted asymmetrically on the vehicle.

		UAS Pitch-Yaw Glideslope Raw Chamber Data						
		Yaw						
		-15°	-10°	-5°	0°	5°	10°	15°
Pitch	15°	-74.9	-74.6	-74.5	-74.5	-74.7	-75.1	-75.7
	10°	-74.6	-74.7	-74.9	-75.2	-75.8	-76.5	-77.6
	5°	-74.6	-74.7	-74.9	-75.3	-75.9	-76.6	-77.5
	0°	-75.6	-75.9	-76.4	-77	-77.7	-78.5	-79.2
	-5°	-75.8	-75.9	-76.2	-76.7	-77.4	-78.2	-79
	-10°	-76.1	-76.1	-76.4	-77	-77.7	-78.5	-79.5
	-15°	-77	-77.1	-77.5	-78.1	-78.9	-79.9	-80.9

Table 5.1 - UAS pitch-yaw glideslope raw chamber data

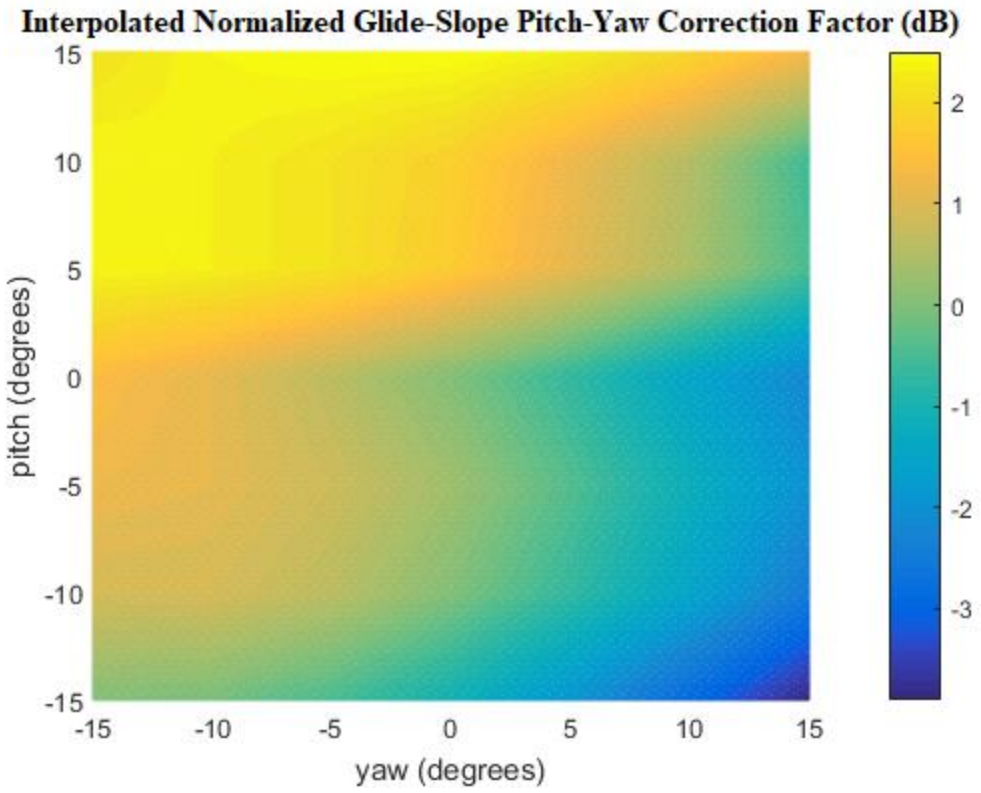

Figure 5.2 - Interpolated normalized glideslope pitch-yaw correction factor (dB)

GPS information can be retrieved from the trigger logs of the UAS controller. These logs are captured every time a trigger signal is sent to the spectrum analyzer. This log contains time, altitude, pitch, roll, yaw, and much more data for the vehicle's condition. From this log pitch and yaw data can be assigned to each channel power measurement. The correction factor can be looked up in figure 5.2 based on each measurement's pitch and yaw. Applying this correction to glideslope horizontal sensitivity data yields figure 5.3. The goal of applying an orientation-based correction to a horizontal sensitivity test would be lowering variance in the measurements. As visible in the previously mentioned figure, variance increased dramatically. This error is not necessarily based on errors in this method or errors in the derived correction factor (figure 5.2).

Figure 5.4 shows the pitch data taken during the glideslope horizontal sensitivity test. Remember from section 4.3 that measurements are taken while the UAS hovers in a stationary position. The relative stability in all horizontal sensitivity measurements seem to indicate that the UAS is

relatively stable while taking measurements. The hypothesis then is that the pitch data itself is the issue. The UAS would not likely be holding in position with such dramatic pitch values. One thought is that there exists a delay in the triggering system that causes the GPS data to be logged either several seconds before or after the measurement is made. Ideally this correction model would be applied to more data sets for testing, but all the applicable trigger logs also contain extreme pitch information.

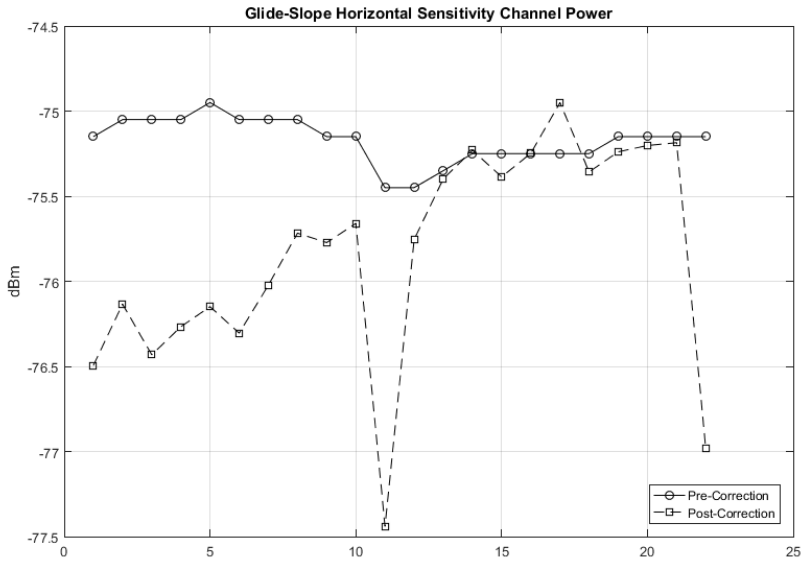

Figure 5.3 - Attempted correction

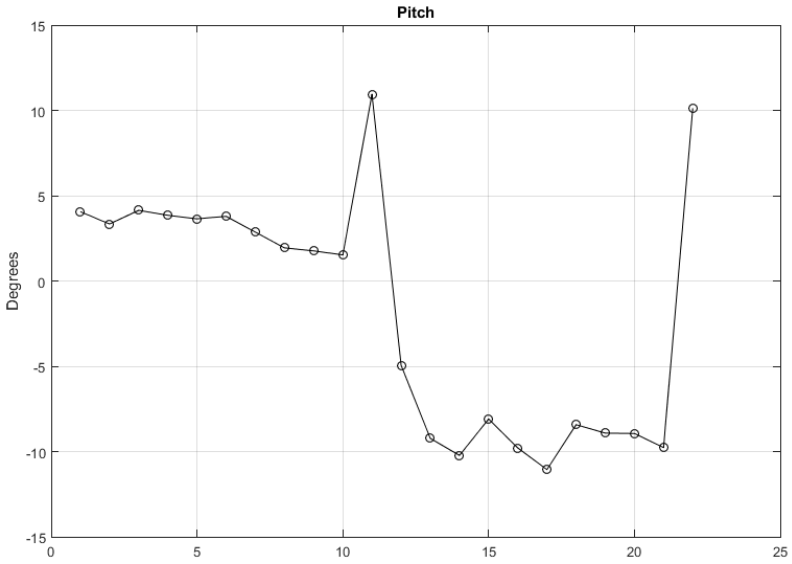

Figure 5.4 - Pitch of flight under correction

CHAPTER VI

CONCLUSION

Based on the empirical data showcased in chapter 4 it seems that this vehicle is capable of inspecting ILS signals with some degree of repeatability. The vertical sensitivities measured indicates the signal power rises and falls over altitude as would be expected. The isotropic sensitivities show the behavior of the receiver antenna as well as the interference from the vehicle chassis. Dipole patterns were witnessed when using dipole receiver and an isotropic pattern was seen in the monopole. Interference from the UAS structure appeared in the DME monopole isotropic sensitivity measurements. Horizontal sensitivity lends some insight into how stable these measurements can be. All the measurements occur at the same altitude and horizontal movement of the UAS should change received channel power very little at this distance from the transmitter. That means any deviation in horizontal sensitivity would be attributed to the vehicle. For localizer this deviation is ±0.1 dB, well within a reasonable tolerance. This deviation was higher in glideslope and DME, leaving room for improvement. After changes were made to the UAS stabilization time, glideslope horizontal sensitivity deviation dropped to ±0.3 dB, ±1 dB for DME. The target performance mentioned by the FAA was ±1.5 dB. This means that although glideslope and DME measurement stability was not as good as localizer, all three ILS were measurable within target specifications.

The theoretical model for EIRxP over altitude generated in chapter 3 can be judged by plotting aside empirical data for chapter 4. These figures are listed in section 4.6. In general, the created model worked well. The localizer model came 10-5 dB below empirical data. As discussed in section 4.6, the diffraction effects incurred from localizer passing through the half-wave ground Fresnel zone are suspect. The glideslope model's arc matches that of the empirical data. It closely follows the data from October and December but sits below the data from June. June glideslope data may be 2 dB higher than in October, December, and model data because of changing atmospheric conditions. Changes in atmosphere moisture content, temperature, and pressure effect atmospheric attenuation as well as refractivity. The DME model floats within all empirical data and possesses the characteristic lobes and regions of destructive interference. The large differences in DME data sets could be from aforementioned atmosphere parameters as well as changes in transmitter orientation.

6.1 – FUTURE WORK

The "month-to-month" repeatability for channel power measurements can be observed in the figures within section 4.5. The differences in data from June to October is generally larger than from October to December. The drift in channel power measurements across the dates could stem from three possible places in the system.

- Change in transmitted power due to alteration in base station location, changed transmitter antenna heading, reassembly of base station, etc.…
- Changes in atmospheric conditions such as atmospheric attenuation or refractivity.
- Changes in losses on the receiver side due to antenna orientations.

More UAS ground testing should be performed to determine if this month-to-month change in received power is caused by it. UAS heading should also be verified. If the UAS is referencing slightly different headings each flight, that could cause the deviation in month-to-month signal strength found.

The theoretical model for EIRxP could be improved as well. Geometric approximations made within the model could be worked out fully. Ground elevation data could be sourced differently. The current data is sourced from the USGS and has a resolution of 1 m and data is taken on the surface every ~25-30 meter. This large area between data points could be negatively impacting the current system of calculating ground reflection points.

The extreme pitch data described in chapter 5 should be investigated. If a delay in the triggering signal is found it should be fixed. The triggering system could be tested at low altitudes by releasing a flag or flashing a light upon trigger. The flag should release, or the light should flash during stabilization.

REFERENCES

[1] National Telecommunications and Information Administration, "Manual of Regulations and Procedures for Federal Radio Frequency Management", 2017, pp. 4.23-4.25.

[2] Rhode & Schwarz Test and Measurement Division, "Operating Manual: Handheld Spectrum Analyzer R&S © FSH". [Online]. Available: https://ieee-dataport.org/sites/default/files/analysis/27/IEEE%20Citation%20Guidelines.pdf. [Accessed: Apr. 10, 2019].

[3] M. P. M. Hall, *Effects of the Troposphere on Radio Communication*, London and New York: The Institution of Electrical Engineers, 1979, pp. 24

[4] S. R. Saunders, *Antennas and Propagation for Wireless Communications Systems*, New Jersey: John Wiley & Sons, 1999, pp. 24-25

[5] J. C. West, "Antennas and Propagation for Wireless Communication Systems – Course Notes", pp. 142-151

[6] K. Siwiak, *Radio Propagation and Antennas for Personal Communications*, MA: Artech House, 1998, pp. 80

[7] K. Siwiak, *Radio Propagation and Antennas for Personal Communications*, MA: Artech House, 1998, pp. 162-163

[8] P. Weckler, personal communication.

[9] A. C. Balanis, *Antenna Theory – Analysis and Design*, New Jersey: John Wiley & Sons, 2016, pp. 319

[10] S. R. Saunders, *Antennas and Propagation for Wireless Communications Systems*, New Jersey: John Wiley & Sons, 1999, pp. 41-42

[11] M. P. M. Hall, "Effects of the Troposphere on Radio Communication", London and New York: The Institution of Electrical Engineers, 1979, pp. 79-92

APPENDICES

APPENDIX A: JUNE FLIGHT CHARACTERISTICS

Flight Name	Flight #	Frequency	Date	Start Time	End Time	Meas# Start	Meas# End
DME Vertical & Isotropic Sensitivity	1	1155 MHz	6/6/2018	830	849	1666	2026
DME Horizontal Sensitivity	2	1155 MHz	6/6/2018	852	907	2027	2328
Glide-Slope Vertical & Isotropic Sensitivity	3	334.7 MHz	6/6/2018	1046	1105	2364	2472
Glide-Slope Horizontal Sensitivity	4	334.7 MHz	6/6/2018	1114	1130	2473	2522
VOR Horizontal Sensitivity	5	108 MHz	6/6/2018	1145	1200	2523	2576
VOR Vertical & Isotropic Sensitivity	6	108 MHz	6/6/2018	1320	1340	2577	2778
LOC Vertical & Isotropic Sensitivity	7	108.1 MHz	6/6/2018	1347	1402	2675	2778
LOC Horizontal Sensitivity	8	108.1 MHz	6/6/2018	1421	1432	2779	2819
DME Power Repeatability 1	9	1155 MHz	6/6/2018	1453	1504	2820	3019
Glide-Slope Power Repeatability 1	10	334.7 MHz	6/6/2018	1511	1515	3020	3036
VOR Power Repeatability 1	11	108 MHz	6/6/2018	1553	1603	3037	3302
LOC Power Repeatability 1	12	108.1 MHz	6/6/2018	1528	1550	3303	3388
DME Power Repeatability 2 (Pre-Amp ON)	13	1155 MHz	6/14/2018	1033	1042	3392	3401
DME Power Repeatability 2 (Pre-Amp OFF)	14	1155 MHz	6/14/2018	1051	1059	3402	3412
Glide-Slope Power Repeatability 2 (Pre-Amp ON)	15	334.7 MHz	6/14/2018	1111	1116	3413	3420
Glide-Slope Power Repeatability 2 (Pre-Amp OFF)	16	334.7 MHz	6/14/2018	1123	1138	3421	3436
VOR Power Repeatability 2	17	108 MHz	6/14/2018	1151	1159	3454	3461
LOC Power Repeatability 2	18	108.1 MHz	6/14/2018	1210	1215	3437	3453
VOR Vertical & Isotropic Sensitivity Retake	19	108 MHz	6/14/2018	1227	1243	3462	3566

Flight Name	Flight #	Triggering Mode			Trigger Logs	Flight Logs	Pre-Amp
		Automated	Manual	Sporadic			
DME Vertical & Isotropic Sensitivity	1			X	NA	Available	ON
DME Horizontal Sensitivity	2			X	NA	Available	ON
Glide-Slope Vertical & Isotropic Sensitivity	3	X			NA	Available	ON
Glide-Slope Horizontal Sensitivity	4	X			NA	NA	ON
VOR Horizontal Sensitivity	5	X			NA	Incomplete	OFF
VOR Vertical & Isotropic Sensitivity	6	X			NA	Incomplete	OFF
LOC Vertical & Isotropic Sensitivity	7	X			NA	Incomplete	OFF
LOC Horizontal Sensitivity	8	X			NA	Incomplete	OFF
DME Power Repeatability 1	9			X	NA	NA	ON
Glide-Slope Power Repeatability 1	10		X		NA	Incomplete	ON
VOR Power Repeatability 1	11			X	NA	NA	OFF
LOC Power Repeatability 1	12			X	NA	NA	OFF
DME Power Repeatability 2 (Pre-Amp ON)	13		X		Available	Available	ON
DME Power Repeatability 2 (Pre-Amp OFF)	14		X		Available	Available	OFF
Glide-Slope Power Repeatability 2 (Pre-Amp ON)	15		X		Available	Available	ON
Glide-Slope Power Repeatability 2 (Pre-Amp OFF)	16		X		Available	Available	OFF
VOR Power Repeatability 2	17		X		Available	Available	OFF
LOC Power Repeatability 2	18		X		Available	Available	OFF
VOR Vertical & Isotropic Sensitivity Retake	19	X			Available	Available	OFF

APPENDIX B: OCTOBER FLIGHT CHARACTERISTICS

Flight Name	Flight #	Frequency	Date	Start Time	End Time	Meas# Start	Meas# End
GBAS Dipole TX Test	1	108.1 MHz	10/26/2018	1318	1328	0	100
LOC Vertical & Isometric Sensitivity	2	108.1 MHz	10/26/2018	1340	1359	101	204
LOC Horizontal Sensitivity	3	108.1 MHz	10/26/2018	1409	1419	205	235
VOR Horizontal Sensitivity	4	108 MHz	10/26/2018	1437	1445	236	256
VOR Vertical & Isometric Sensitivity	5	108 MHz	10/26/2018	1602	1644	257	362
Glide-Slope Vertical & Isometric Sensitivity	6	334.7 MHz	10/26/2018	1658	1710	363	467
Glide-Slope Horizontal Sensitivity	7	334.7 MHz	10/26/2018	1737	1746	468	498
DME Vertical & Isometric Sensitivity	8	1155 MHz	10/26/2018	1821	1835	499	605
DME Horizontal Sensitivity	9	1155 MHz	10/26/2018	1846	1856	606	637

Flight Name	Flight #	Triggering Mode			Trigger Logs	Flight Logs	Pre-Amp
		Automated	Manual	Sporatic			
GBAS Dipole TX Test	1	X			Available	Available	OFF
LOC Vertical & Isometric Sensitivity	2	X			Available	Available	OFF
LOC Horizontal Sensitivity	3	X			Available	Available	OFF
VOR Horizontal Sensitivity	4	X			Available	Available	OFF
VOR Vertical & Isometric Sensitivity	5	X			Available	Available	OFF
Glide-Slope Vertical & Isometric Sensitivity	6	X			Available	Available	OFF
Glide-Slope Horizontal Sensitivity	7	X			Available	Available	OFF
DME Vertical & Isometric Sensitivity	8	X			Polluted	Available	OFF
DME Horizontal Sensitivity	9	X			Polluted	Available	OFF

APPENDIX C: DECEMBER FLIGHT CHARACTERISTICS

Flight Name	Flight #	Frequency	Date	Start Time	End Time	Meas# Start	Meas# End
LOC Vertical & Isometric Sensitivity	1	108.1 MHz	12/21/2018	1103	1120	0	104
LOC Horizontal Sensitivity	2	108.1 MHz	12/21/2018	1128	1141	105	127
Glide-Slope Vertical & Isometric Sensitivity	3	334.7 MHz	12/21/2018	1145	1202	128	232
Glide-Slope Horizontal Sensitivity	4	334.7 MHz	12/21/2018	1253	1307	233	257
DME Vertical & Isometric Sensitivity	5	1155 MHz	12/21/2018	1318	1334	258	364
DME Horizontal Sensitivity	6	1155 MHz	12/21/2018	1338	1352	365	390
VOR Horizontal Sensitivity [EVSF1000]	7	108 MHz	12/21/2018	1418	1432	NA	900
VOR Vertical & Isometric Sensitivity [EVSF1000]	8	108 MHz	12/21/2018	1449	1459	NA	738
LOC Horizontal Sensitivity [EVSF1000]	9	108.1 MHz	12/21/2018	1512	1525	NA	889

Flight Name	Flight #	Triggering Mode			Trigger Logs	Flight Logs	Pre-Amp
		Automated	Manual	Sporatic			
LOC Vertical & Isometric Sensitivity	1	X			Available	Available	OFF
LOC Horizontal Sensitivity	2	X			Available	Available	OFF
Glide-Slope Vertical & Isometric Sensitivity	3	X			Available	Available	OFF
Glide-Slope Horizontal Sensitivity	4	X			Available	Available	OFF
DME Vertical & Isometric Sensitivity	5	X			Available	Available	OFF
DME Horizontal Sensitivity	6	X			Available	Available	OFF
VOR Horizontal Sensitivity [EVSF1000]	7	X			Available	Available	NA
VOR Vertical & Isometric Sensitivity [EVSF1000]	8	X			NA	Available	NA
LOC Horizontal Sensitivity [EVSF1000]	9	X			Available	Available	NA

APPENDIX D: LOCALIZER MODEL MATLAB CODE

```
% --- Loading/Saving USGS Elevation Data ---
%[TuttleElevationData lat lon]=mapreader2('tuttle.dt2');
%save('TuttleElevationData.mat','TuttleElevationData')
%save('lat.mat','lat')
load('TuttleElevationData.mat','TuttleElevationData')
load('lat.mat','lat')
lon = -98:1/3600:-97;

% --- Basic Transmission Parameters ---
f = 108e6;
fMHz = f*1e-6;
c = 2.998e8;
llambda = c/f;
distance = 19430;
%Ground Fresnel Zone
GFZ = 2;

% --- Grazing Angles ---
alpha = 0:0.00001:pi/2;
alphaDeg = alpha*180/pi;

% --- Standard Earth Radius ---
r0 = 6.366e6;
% --- Standard Refractivity ---
A = 3.9e-8;
% --- Effective Earth Radius ---
K = 4/3;
a = K * r0;

% --- Relative Permittivity of Ground ---
sigma = 0.1;
epsilon0 = 8.854187817e-12;
epsilong = 10 - (i*sigma)/(epsilon0*2*pi*f);

% --- Initial Launch Angle of Atmosphere with Standard Refractivity ---
h_m = ((distance/2)^2)/(2*a);
A_prime = A - (1 / r0);
alpha_0 = sqrt(abs(h_m * 2 * A_prime));

% --- Geometry ---
TXheight = 5.5;
RXheightFT = 500:10:1600;
RXheight = RXheightFT./3.28084;
alpha2 = atan(RXheight./distance) + alpha_0;
TXheightFT = 3.28084* TXheight;
RXheightFTRayModel = [500 1500 1600];
RXheightRayModel = RXheightFTRayModel./3.28084;

% --- Plotting Elevation Heat Map ---
figure('Renderer', 'painters', 'Position', [700 200 900 600])
imagesc(lon,lat,TuttleElevationData);
set(gca,'ydir','normal')
```

```
axis equal
grid on
hold
plot([-97.809114 -97.626944], [35.295686 35.386667],'--ok')
xlabel('Longitude (decimal degrees)')
ylabel('Latitude (decimal degrees)')
title('Digital Terrain Elevation Data for MMAC -> THS Propagation
Path')

towersXindex = [round((1 - 0.626944)*3600) round((1 - 0.809114)*3600)];
towersYindex = [round(0.386667*3600) round(0.295686*3600)];

% --- Link Calculations and Plotting ---
rLLink = zeros(1,length(towersXindex)-1);
linkPhi = zeros(1,length(towersXindex)-1);
linkDistance = zeros(1,length(towersXindex)-1);
dXLink = towersXindex(2)-towersXindex(1);
dYLink = towersYindex(2)-towersYindex(1);
dLLink = sqrt(dXLink^2 + dYLink^2);
rLLink(1) = round(dLLink);
linkPhi(1) = atan(dYLink / dXLink);
for n = 0:rLLink(1)
    elevLink(n+1) = TuttleElevationData((1 + towersYindex(1) +
round(dYLink*n/rLLink(1))), 1 + towersXindex(1) +
round(dXLink*n/rLLink(1)));
    rhoLink(n+1) = sqrt((25.3*dXLink*n/rLLink(1))^2 +
(30.8*dYLink*n/rLLink(1))^2);
end
linkDistance(1) = rhoLink(end);

% --- LOS Paths ---
rhoTX = rhoLink(1);
rhoRX = rhoLink(end);
elevTX = elevLink(1)+ TXheight;
elevRX = elevLink(end)+ RXheightRayModel;

% --- Clearances ---
halfLinkDistance = linkDistance(1)/2;
curve = ((halfLinkDistance^2) - (abs(halfLinkDistance - rhoLink).^2)) /
(2*a);
elevLink = elevLink + curve;
trees2 = elevLink + 1;
Fresnel2 = trees2 + sqrt(0.5*llambda*(linkDistance(1)-
rhoLink).*rhoLink/linkDistance(1));

% --- Creation of a Higher Resolution elevLink & rhoLink via
Interpolation
InterScale = 100;
for i = 1:length(elevLink)-1
    for j = 1:InterScale
        k = ((i-1)*100)+j;
        rhoLinkHD(k) = rhoLink(i) + ((rhoLink(i+1)-
rhoLink(i))*j/InterScale);
        elevLinkHD(k) =elevLink(i) + ((elevLink(i+1)-
elevLink(i))*j/InterScale);
    end
```

```
end
curveHD = ((halfLinkDistance^2) - (abs(halfLinkDistance -
rhoLinkHD).^2)) / (2*a);
elevLinkHD = elevLinkHD + curveHD;

% --- Finding Reflections ---
reflectionTolerence = 10;
for m = 1:length(RXheight)
    reflectionTolerence = 1;
    for n = 2:(length(rhoLinkHD)-1)
        alphaN = atan((TXheight + elevLink(1) -
elevLinkHD(n))/rhoLinkHD(n));
        rayEndAlt = elevLinkHD(n) + (rhoLink(end)-
rhoLinkHD(n))*tan(alphaN);
        if abs(RXheight(m) + elevLink(end) - rayEndAlt) <
reflectionTolerence
            rhoRefl(m) = rhoLinkHD(n);
            elevRefl(m) = elevLinkHD(n);
            indexRefl(m) = n;
            reflectionTolerence = abs(RXheight(m) + elevLink(end) -
rayEndAlt);
        end
    end
end

% --- RMS Elevation over Reflection Region ---
sigma_front_s = std(elevLinkHD(1500:6400));
rayCrit = sigma_front_s * sin(max(alpha2));
rayCritMet = false;
if(rayCrit < (llambda/8))
    rayCritMet = true;
end

% --- Gridlines ---
grida = zeros(1,length(elevLink)) + curve + 400;
gridb = zeros(1,length(elevLink)) + curve + 600;
gridc = zeros(1,length(elevLink)) + curve + 800;

% --- Reflection Ray Figures ---
for n = 1:10:length(RXheight)
    figure('Renderer', 'painters', 'Position', [700 200 900 600])
    plot([rhoTX rhoRX],[elevTX (RXheight(n)+elevLink(end))],'k',[rhoTX
rhoRefl(n) rhoRX],[elevTX elevRefl(n) (RXheight(n)+elevLink(end))],'--
k')
    hold
    plot(rhoLink,elevLink,'b',rhoLink,trees2,'--g',rhoLink,Fresnel2,'--
r')
    plot(rhoLink,grida,':k',rhoLink,gridb,':k',rhoLink,gridc,':k')
    title(['Propagation Path; f = ',num2str(fMHz),' MHz\newlineTX
Height: ',num2str(TXheight),'m (',num2str(TXheight*3.28084),' ft), RX
Height: ',num2str(RXheight(n)),'m (',num2str(RXheight(n)*3.28084),' ft)
[AGL]']);
    xlabel('Distance from TX (m) - rho~x')
    ylabel('Elevation MSL (m) - z')
    legend('Line-of-Sight Ray','Ground Reflection','Ground','Tree
Allowance','108 MHz Half-Fresnel Clearance','location','southoutside')
```

```
end

% --- Gamma ---
Xh = sqrt(epsilong - (cos(alpha)).^2);
Gamma = (sin(alpha) - Xh)./(sin(alpha) + Xh);
GammaAbs = abs(Gamma);
%-------------------------
Xh2 = sqrt(epsilong - (cos(alpha2)).^2);
Gamma2 = (sin(alpha2) - Xh2)./(sin(alpha2) + Xh2);
GammaAbs2 = abs(Gamma2);

% --- Gamma Figures ---
figure('Renderer', 'painters', 'Position', [700 200 900 600])
plot(alphaDeg, real(Gamma),'--k', alphaDeg, imag(Gamma),':k', alphaDeg,
GammaAbs,'k')
title('Ground Reflection Coefficient for Horizontal Polarization,
\newline\Gamma(\alpha), \epsilon_g = 10, \sigma_g = 0.1')
ylabel('\Gamma')
xlabel('Grazing Angle \alpha (degrees)')
legend('\Gamma real','\Gamma
imaginary','|\Gamma|','location','southoutside')
grid on

% --- Roughness Factor ---
RF = exp(-0.5*((4*pi*sigma_front_s*sin(alpha)/llambda).^2));
RF2 = exp(-0.5*((4*pi*sigma_front_s.*sin(alpha2)/llambda).^2));

% --- Roughness Factor Plot ---
figure('Renderer', 'painters', 'Position', [700 200 900 600])
plot(alphaDeg,RF,'k')
title(['Roughness Factor: \sigma_s = ',num2str(sigma_front_s),', f =
',num2str(f * 1e-6),' MHz'])
grid on
xlabel('Grazing Angle \alpha (degrees)')
ylabel('Roughness Factor')

% --- Fine Roughness Factor Plot ---
figure('Renderer', 'painters', 'Position', [700 200 900 600])
plot(alphaDeg(1:16000),RF(1:16000),'k')
title(['Roughness Factor: \sigma_s = ',num2str(sigma_front_s),', f =
',num2str(f * 1e-6),' MHz'])
grid on
xlabel('Grazing Angle \alpha (degrees)')
ylabel('Roughness Factor')

% --- Divergence Factor ---
DF = 1./sqrt(1 + (2.*rhoRefl.*(rhoLink(end) -
rhoRefl))./(a.*rhoLink(end).*tan(alpha2)));
DFdB = 20.*log10(DF);
max(DFdB)
min(DFdB)

% --- Polar Array Factor ---
AF = abs(1 + Gamma.*cos(4*pi*TXheight*sin(alpha)/llambda));
AF = 20*log10(AF);
```

```
%------------------------
AFclip = AF;
AFclip(AFclip < -40) = -40;

% --- Polar Array Factor Figure ---
figure('Renderer', 'painters', 'Position', [700 200 900 600])
polarplot(alpha,AFclip,'k')
title('Localizer Reflection Pattern (dB)')
rlim([-40 10])
thetalim([0 90])
grid minor

% --- Rectangular Array Factor (With Roughness Factor) ---
AF2 = abs(1 + Gamma2.*cos(4*pi*TXheight*sin(alpha2)/llambda));
AF2 = 20*log10(AF2);

% --- Rectangular Array Factor Plot ---
figure('Renderer', 'painters', 'Position', [700 200 900 600])
plot(RXheightFT,AF2,'k')
title('Localizer Reflection Pattern vs Altitude')
ylabel('Gain (dB)')
xlabel('Altitude (ft)')
grid on

% --- Transmit power (dBm), transmitter gain (dBi), & path loss (dB) --
-
TXpower = 17.4 - 1.4;
TXAntGain = 11.0;
PL = 20*log10(llambda/(4*pi*distance));

% --- Equivalent Isotropic Reciever Power ---
EIRxP = AF2 + TXpower + TXAntGain + PL;

% --- EIRxP Figure ---
figure('Renderer', 'painters', 'Position', [700 200 900 600])
plot(RXheightFT,EIRxP,'k')
title('Localizer EIRxP vs Altitude')
ylabel('EIRxP (dBm)')
xlabel('Altitude (ft)')
grid on
```

APPENDIX E: GLIDESLOPE MODEL MATLAB CODE

```
% --- Loading/Saving USGS Elevation Data ---
%[TuttleElevationData lat lon]=mapreader2('tuttle.dt2');
%save('TuttleElevationData.mat','TuttleElevationData')
%save('lat.mat','lat')
load('TuttleElevationData.mat','TuttleElevationData')
load('lat.mat','lat')
lon = -98:1/3600:-97;

% --- Import Imperical Data ---
VertIso = csvread('Dec_FSH_VertIso.csv');

% --- Knowns ---
f = 334.7e6;
fMHz = f*1e-6;
c = 2.998e8;
llambda = c/f;
distance = 19430;

% --- Grazing Angles ---
alpha = 0:0.00001:pi/2;
alphaDeg = alpha*180/pi;

% --- Standard Earth Radius ---
r0 = 6.366e6;
% --- Standard Refractivity ---
A = 3.9e-8;
% --- Effective Earth Radius ---
K = 4/3;
a = K * r0;

% --- Relative Permittivity of Ground ---
sigma = 0.1;
epsilon0 = 8.854187817e-12;
epsilong = 10 - (i*sigma)/(epsilon0*2*pi*f);

% --- Initial Launch Angle of Atmosphere with Standard Refractivity ---
h_m = ((distance/2)^2)/(2*a);
A_prime = A - (1 / r0);
alpha_0 = sqrt(abs(h_m * 2 * A_prime));

% --- Geometry ---
TXheight = 8.6;
RXheightFT = 500:10:1600;
RXheight = RXheightFT./3.28084;
alpha2 = atan(RXheight./distance) + alpha_0;
TXheightFT = 3.28084* TXheight;
RXheightFTRayModel = [500 1500 1600];
RXheightRayModel = RXheightFTRayModel./3.28084;

% --- Plotting Elevation Heat Map ---
figure('Renderer', 'painters', 'Position', [700 200 900 600])
imagesc(lon,lat,TuttleElevationData);
```

```
set(gca,'ydir','normal')
axis equal
grid on
hold
plot([-97.809114 -97.626944], [35.295686 35.386667],'--ok')
xlabel('Longitude (decimal degrees)')
ylabel('Latitude (decimal degrees)')
title('Digital Terrain Elevation Data for MMAC -> THS Propagation
Path')

towersXindex = [round((1 - 0.626944)*3600) round((1 - 0.809114)*3600)];
towersYindex = [round(0.386667*3600) round(0.295686*3600)];

% --- Link Calculations and Plotting ---
rLLink = zeros(1,length(towersXindex)-1);
linkPhi = zeros(1,length(towersXindex)-1);
linkDistance = zeros(1,length(towersXindex)-1);
dXLink = towersXindex(2)-towersXindex(1);
dYLink = towersYindex(2)-towersYindex(1);
dLLink = sqrt(dXLink^2 + dYLink^2);
rLLink(1) = round(dLLink);
linkPhi(1) = atan(dYLink / dXLink);
for n = 0:rLLink(1)
    elevLink(n+1) = TuttleElevationData((1 + towersYindex(1) +
round(dYLink*n/rLLink(1))), 1 + towersXindex(1) +
round(dXLink*n/rLLink(1)));
    rhoLink(n+1) = sqrt((25.3*dXLink*n/rLLink(1))^2 +
(30.8*dYLink*n/rLLink(1))^2);
end
linkDistance(1) = rhoLink(end);

% --- LOS Paths ---
rhoTX = rhoLink(1);
rhoRX = rhoLink(end);
elevTX = elevLink(1)+ TXheight;
elevRX = elevLink(end)+ RXheightRayModel;

% --- Clearances ---
halfLinkDistance = linkDistance(1)/2;
curve = ((halfLinkDistance^2) - (abs(halfLinkDistance - rhoLink).^2)) /
(2*a);
elevLink = elevLink + curve;
trees2 = elevLink + 1;
Fresnel2 = trees2 + sqrt(0.5*llambda*(linkDistance(1)-
rhoLink).*rhoLink/linkDistance(1));

% --- Creation of a Higher Resolution elevLink & rhoLink via
Interpolation
InterScale = 100;
for i = 1:length(elevLink)-1
    for j = 1:InterScale
        k = ((i-1)*100)+j;
        rhoLinkHD(k) = rhoLink(i) + ((rhoLink(i+1)-
rhoLink(i))*j/InterScale);
        elevLinkHD(k) =elevLink(i) + ((elevLink(i+1)-
elevLink(i))*j/InterScale);
```

```
    end
end
curveHD = ((halfLinkDistance^2) - (abs(halfLinkDistance -
rhoLinkHD).^2)) / (2*a);
elevLinkHD = elevLinkHD + curveHD;

% --- Finding Reflections ---
reflectionTolerence = 10;
for m = 1:length(RXheight)
    reflectionTolerence = 1;
    for n = 2:(length(rhoLinkHD)-1)
        alphaN = atan((TXheight + elevLink(1) -
elevLinkHD(n))/rhoLinkHD(n));
        rayEndAlt = elevLinkHD(n) + (rhoLink(end)-
rhoLinkHD(n))*tan(alphaN);
        if abs(RXheight(m) + elevLink(end) - rayEndAlt) <
reflectionTolerence
            rhoRefl(m) = rhoLinkHD(n);
            elevRefl(m) = elevLinkHD(n);
            indexRefl(m) = n;
            reflectionTolerence = abs(RXheight(m) + elevLink(end) -
rayEndAlt);
        end
    end
end

% --- RMS Elevation over Reflection Region ---
sigma_front_s = std(elevLinkHD(1500:6400));
rayCrit = sigma_front_s * sin(max(alpha2));
rayCritMet = false;
if(rayCrit < (llambda/8))
    rayCritMet = true;
end

% --- Gridlines ---
grida = zeros(1,length(elevLink)) + curve + 400;
gridb = zeros(1,length(elevLink)) + curve + 600;
gridc = zeros(1,length(elevLink)) + curve + 800;

% --- Reflection Ray Figures ---
for n = 1:10:length(RXheight)
    figure('Renderer', 'painters', 'Position', [700 200 900 600])
    plot([rhoTX rhoRX],[elevTX (RXheight(n)+elevLink(end))],'k',[rhoTX
rhoRefl(n) rhoRX],[elevTX elevRefl(n) (RXheight(n)+elevLink(end))],'--
k')
    hold
    plot(rhoLink,elevLink,'b',rhoLink,trees2,'--g',rhoLink,Fresnel2,'--
r')
    plot(rhoLink,grida,':k',rhoLink,gridb,':k',rhoLink,gridc,':k')
    title(['Propagation Path; f = ',num2str(fMHz),' MHz\newlineTX
Height: ',num2str(TXheight),'m (',num2str(TXheight*3.28084),' ft), RX
Height: ',num2str(RXheight(n)),'m (',num2str(RXheight(n)*3.28084),' ft)
[AGL]']);
    xlabel('Distance from TX (m) - rho~x')
    ylabel('Elevation MSL (m) - z')
```

```
    legend('Line-of-Sight Ray','Ground Reflection','Ground','Tree
Allowance','334.7 MHz Half-Fresnel
Clearance','location','southoutside')
end

% --- Gamma ---
Xh = sqrt(epsilong - (cos(alpha)).^2);
Gamma = (sin(alpha) - Xh)./(sin(alpha) + Xh);
GammaAbs = abs(Gamma);
%-------------------------
Xh2 = sqrt(epsilong - (cos(alpha2)).^2);
Gamma2 = (sin(alpha2) - Xh2)./(sin(alpha2) + Xh2);
GammaAbs2 = abs(Gamma2);

% --- Gamma Figures ---
figure('Renderer', 'painters', 'Position', [700 200 900 600])
plot(alphaDeg, real(Gamma),'--k', alphaDeg, imag(Gamma),':k', alphaDeg,
GammaAbs,'k')
title('Ground Reflection Coefficient for Horizontal Polarization,
\newline\Gamma(\alpha), \epsilon_g = 10, \sigma_g = 0.1')
ylabel('\Gamma')
xlabel('Grazing Angle \alpha (degrees)')
legend('\Gamma real','\Gamma
imaginary','|\Gamma|','location','southoutside')
grid on

% --- Gamma Figure 2 ---
figure('Renderer', 'painters', 'Position', [700 200 900 600])
plot(alphaDeg, GammaAbs, 'k')
title('Ground Reflection Coefficient for Horizontal Polarization,
\newline\epsilon_r = 10, \sigma_g = 0.1')
ylabel('|\Gamma(\alpha)|')
xlabel('Grazing Angle \alpha (degrees)')
grid on
ylim([0 1])

% --- Roughness Factor ---
RF = exp(-0.5*((4*pi*sigma_front_s.*sin(alpha)/llambda).^2));
RF2 = exp(-0.5*((4*pi*sigma_front_s.*sin(alpha2)/llambda).^2));

% --- Roughness Factor Plot ---
figure('Renderer', 'painters', 'Position', [700 200 900 600])
plot(alphaDeg,RF,'k')
title(['Roughness Factor: \sigma_s = ',num2str(sigma_front_s),', f =
',num2str(f * 1e-6),' MHz'])
grid on
xlabel('Grazing Angle \alpha (degrees)')
ylabel('Roughness Factor')

% --- Fine Roughness Factor Plot ---
figure('Renderer', 'painters', 'Position', [700 200 900 600])
plot(alphaDeg(1:16000),RF(1:16000),'k')
title(['Roughness Factor: \sigma_s = ',num2str(sigma_front_s),', f =
',num2str(f * 1e-6),' MHz'])
grid on
xlabel('Grazing Angle \alpha (degrees)')
```

```
ylabel('Roughness Factor')

% --- Polar Array Factor ---
AF = abs(1 + Gamma.*cos(4*pi*TXheight*sin(alpha)/llambda));
AF = 20*log10(AF);
%-----------------------
AFclip = AF;
AFclip(AFclip < -40) = -40;

% --- Polar Array Factor Figure ---
figure('Renderer', 'painters', 'Position', [700 200 900 600])
polarplot(alpha,AFclip,'k')
title('Glide-Slope Reflection Pattern (dB)')
rlim([-40 10])
thetalim([0 90])
grid minor

% --- Rectangular Array Factor (With Roughness Factor) ---
AF2 = abs(1 + Gamma2.*cos(4*pi*TXheight*sin(alpha2)/llambda));
AF2 = 20*log10(AF2);

% --- Rectangular Array Factor Plot ---
figure('Renderer', 'painters', 'Position', [700 200 900 600])
plot(RXheightFT,AF2,'k')
title('Glide-Slope Reflection Pattern vs Altitude')
ylabel('Gain (dB)')
xlabel('Altitude (ft)')
grid on

% --- Transmit power (dBm), transmitter gain (dBi), & path loss (dB) --
-
TXpower = 17 - 1.9;
TXAntGain = 11.1;
PL = 20*log10(llambda/(4*pi*distance));

% --- Equivalent Isotropic Reciever Power ---
EIRxP = AF2 + TXpower + TXAntGain + PL;

% --- EIRxP Figure ---
figure('Renderer', 'painters', 'Position', [700 200 900 600])
plot(RXheightFT,EIRxP,'k')
title('Glide-Slope EIRxP vs Altitude')
ylabel('EIRxP (dBm)')
xlabel('Altitude (ft)')
grid on
```

APPENDIX F: DME MODEL MATLAB CODE

```
% --- Loading/Saving USGS Elevation Data ---
%[TuttleElevationData lat lon]=mapreader2('tuttle.dt2');
%save('TuttleElevationData.mat','TuttleElevationData')
%save('lat.mat','lat')
load('TuttleElevationData.mat','TuttleElevationData')
load('lat.mat','lat')
lon = -98:1/3600:-97;

% --- Import Imperical Data
VertIso = csvread('Dec_FSH_VertIso.csv');

% --- Knowns
f = 1155e6;
fMHz = f*1e-6;
c = 2.998e8;
llambda = c/f;
distance = 19430;

% --- Grazing Angles ---
alpha = 0:0.00001:pi/2;
alphaDeg = alpha*180/pi;

% --- Standard Earth Radius ---
r0 = 6.366e6;
% --- Standard Refractivity ---
A = 3.9e-8;
% --- Effective Earth Radius ---
K = 4/3;
a = K * r0;

% --- Relative Permittivity of Ground ---
sigma = 0.1;
epsilon0 = 8.854187817e-12;
epsilong = 10 - (i*sigma)/(epsilon0*2*pi*f);

% --- Initial Launch Angle of Atmosphere with Standard Refractivity ---
h_m = ((distance/2)^2)/(2*a);
A_prime = A - (1 / r0);
alpha_0 = sqrt(abs(h_m * 2 * A_prime));

% --- Geometry ---
TXheight = 9.85;
RXheightFT = 500:10:1600;
RXheight = RXheightFT./3.28084;
alpha2 = atan(RXheight./distance) + alpha_0;
TXheightFT = 3.28084* TXheight;
RXheightFTRayModel = [500 1500 1600];
RXheightRayModel = RXheightFTRayModel./3.28084;

% --- Plotting Elevation Heat Map ---
figure('Renderer', 'painters', 'Position', [700 200 900 600])
```

```
imagesc(lon,lat,TuttleElevationData);
set(gca,'ydir','normal')
axis equal
grid on
hold
plot([-97.809114 -97.626944], [35.295686 35.386667],'--ok')
xlabel('Longitude (decimal degrees)')
ylabel('Latitude (decimal degrees)')
title('Digital Terrain Elevation Data for MMAC -> THS Propagation
Path')

towersXindex = [round((1 - 0.626944)*3600) round((1 - 0.809114)*3600)];
towersYindex = [round(0.386667*3600) round(0.295686*3600)];

% --- Link Calculations and Plotting ---
rLLink = zeros(1,length(towersXindex)-1);
linkPhi = zeros(1,length(towersXindex)-1);
linkDistance = zeros(1,length(towersXindex)-1);
dXLink = towersXindex(2)-towersXindex(1);
dYLink = towersYindex(2)-towersYindex(1);
dLLink = sqrt(dXLink^2 + dYLink^2);
rLLink(1) = round(dLLink);
linkPhi(1) = atan(dYLink / dXLink);
for n = 0:rLLink(1)
    elevLink(n+1) = TuttleElevationData((1 + towersYindex(1) +
round(dYLink*n/rLLink(1))), 1 + towersXindex(1) +
round(dXLink*n/rLLink(1)));
    rhoLink(n+1) = sqrt((25.3*dXLink*n/rLLink(1))^2 +
(30.8*dYLink*n/rLLink(1))^2);
end
linkDistance(1) = rhoLink(end);

% --- LOS Paths ---
rhoTX = rhoLink(1);
rhoRX = rhoLink(end);
elevTX = elevLink(1)+ TXheight;
elevRX = elevLink(end)+ RXheightRayModel;

% --- Clearances ---
halfLinkDistance = linkDistance(1)/2;
curve = ((halfLinkDistance^2) - (abs(halfLinkDistance - rhoLink).^2)) /
(2*a);
elevLink = elevLink + curve;
trees2 = elevLink + 1;
Fresnel2 = trees2 + sqrt(0.5*llambda*(linkDistance(1)-
rhoLink).*rhoLink/linkDistance(1));

% --- Creation of a Higher Resolution elevLink & rhoLink via
Interpolation
InterScale = 100;
for i = 1:length(elevLink)-1
    for j = 1:InterScale
        k = ((i-1)*100)+j;
        rhoLinkHD(k) = rhoLink(i) + ((rhoLink(i+1)-
rhoLink(i))*j/InterScale);
```

```
        elevLinkHD(k) = elevLink(i) + ((elevLink(i+1)-
elevLink(i))*j/InterScale);
    end
end
curveHD = ((halfLinkDistance^2) - (abs(halfLinkDistance -
rhoLinkHD).^2)) / (2*a);
elevLinkHD = elevLinkHD + curveHD;

% --- Finding Reflections ---
reflectionTolerence = 10;
for m = 1:length(RXheight)
    reflectionTolerence = 1;
    for n = 2:(length(rhoLinkHD)-1)
        alphaN = atan((TXheight + elevLink(1) -
elevLinkHD(n))/rhoLinkHD(n));
        rayEndAlt = elevLinkHD(n) + (rhoLink(end)-
rhoLinkHD(n))*tan(alphaN);
        if abs(RXheight(m) + elevLink(end) - rayEndAlt) <
reflectionTolerence
            rhoRefl(m) = rhoLinkHD(n);
            elevRefl(m) = elevLinkHD(n);
            indexRefl(m) = n;
            reflectionTolerence = abs(RXheight(m) + elevLink(end) -
rayEndAlt);
        end
    end
end

% --- RMS Elevation over Reflection Region ---
sigma_front_s = std(elevLinkHD(1500:6400));
rayCrit = sigma_front_s * sin(max(alpha2));
rayCritMet = false;
if(rayCrit < (llambda/8))
    rayCritMet = true;
end

% --- Gridlines ---
grida = zeros(1,length(elevLink)) + curve + 400;
gridb = zeros(1,length(elevLink)) + curve + 600;
gridc = zeros(1,length(elevLink)) + curve + 800;

% --- Reflection Ray Figures ---
for n = 1:10:length(RXheight)
    figure('Renderer', 'painters', 'Position', [700 200 900 600])
    plot([rhoTX rhoRX],[elevTX (RXheight(n)+elevLink(end))],'k',[rhoTX
rhoRefl(n) rhoRX],[elevTX elevRefl(n) (RXheight(n)+elevLink(end))],'--
k')
    hold
    plot(rhoLink,elevLink,'b',rhoLink,trees2,'--g',rhoLink,Fresnel2,'--
r')
    plot(rhoLink,grida,':k',rhoLink,gridb,':k',rhoLink,gridc,':k')
    title(['Propagation Path; f = ',num2str(fMHz),' MHz\newlineTX
Height: ',num2str(TXheight),'m (',num2str(TXheight*3.28084),' ft), RX
Height: ',num2str(RXheight(n)),'m (',num2str(RXheight(n)*3.28084),' ft)
[AGL]']);
    xlabel('Distance from TX (m) - rho~x')
```

```
    ylabel('Elevation MSL (m) - z')
    legend('Line-of-Sight Ray','Ground Reflection','Ground','Tree
Allowance','1155 MHz Half-Fresnel Clearance','location','southoutside')
end

% --- Gamma ---
Xv = sqrt((epsilong - (cos(alpha)).^2))./epsilong;
Gamma = (sin(alpha) - Xv)./(sin(alpha) + Xv);
GammaAbs = abs(Gamma);
%---------------------------------------
Xv2 = sqrt(epsilong - (cos(alpha2)).^2)./epsilong;
Gamma2 = (sin(alpha2) - Xv2)./(sin(alpha2) + Xv2);
GammaAbs2 = abs(Gamma2);

% --- Roughness Factor ---
RF = exp(-0.5*((4*pi*sigma_front_s*sin(alpha)/llambda).^2));
RF2 = exp(-0.5*((4*pi*sigma_front_s.*sin(alpha2)/llambda).^2));

% --- Gamma Figure ---
figure('Renderer', 'painters', 'Position', [700 200 900 600])
plot(alphaDeg, real(Gamma),'--k', alphaDeg, imag(Gamma),':k', alphaDeg,
GammaAbs,'k')
title('Ground Reflection Coefficient for Vertical Polarization,
\newline\Gamma(\alpha), \epsilon_g = 10, \sigma_g = 0.1')
ylabel('\Gamma')
xlabel('Grazing Angle \alpha (degrees)')
legend('\Gamma real','\Gamma
imaginary','|\Gamma|','location','southoutside')
grid on

% --- Gamma Figure 2 ---
figure('Renderer', 'painters', 'Position', [700 200 900 600])
plot(alphaDeg, GammaAbs, 'k')
title('Ground Reflection Coefficient for Vertical Polarization,
\newline\epsilon_r = 10, \sigma_g = 0.1')
ylabel('|\Gamma(\alpha)|')
xlabel('Grazing Angle \alpha (degrees)')
grid on
ylim([0 1])

% --- Roughness Factor Plot ---
figure('Renderer', 'painters', 'Position', [700 200 900 600])
plot(alphaDeg,RF,'k')
title(['Roughness Factor: \sigma_s = ',num2str(sigma_front_s),', f =
',num2str(f * 1e-6),' MHz'])
grid on
xlabel('Grazing Angle \alpha (degrees)')
ylabel('Roughness Factor')

% --- Fine Roughness Factor Plot ---
figure('Renderer', 'painters', 'Position', [700 200 900 600])
plot(alphaDeg(1:16000),RF(1:16000),'k')
title(['Roughness Factor: \sigma_s = ',num2str(sigma_front_s),', f =
',num2str(f * 1e-6),' MHz'])
grid on
xlabel('Grazing Angle \alpha (degrees)')
```

```
ylabel('Roughness Factor')

% --- Polar Array Factor ---
AF = abs(1 - Gamma.*cos(4*pi*TXheight*sin(alpha)/llambda));
AF = 20*log10(AF);
%-----------------------
AFclip = AF;
AFclip(AFclip < -40) = -40;

% --- Polar Array Factor Plot ---
figure('Renderer', 'painters', 'Position', [700 200 900 600])
polarplot(alpha,AFclip,'k')
title('DME Reflection Pattern (dB)')
rlim([-40 10])
thetalim([0 90])
grid minor

% --- Rectangular Array Factor (With Roughness Factor) ---
AF2 = abs(1 - RF2.*Gamma2.*cos(4*pi*TXheight*sin(alpha2)/llambda));
AF2 = 20*log10(AF2);

% --- Rectangular Array Factor ---
figure('Renderer', 'painters', 'Position', [700 200 900 600])
plot(RXheightFT,AF2,'k')
title('DME Reflection Pattern vs Altitude')
ylabel('Gain (dB)')
xlabel('Altitude (ft)')
grid on

% --- Transmit power (dBm), transmitter gain (dBi), & path loss (dB) --
-
TXpower = 37 - 3.8;
TXAntGain = 7.1;
PL = 20*log10(llambda/(4*pi*distance));

% --- Equivalent Isotropic Reciever Power ---
EIRxP = AF2 + TXpower + TXAntGain + PL;

% --- EIRxP Figure ---
figure('Renderer', 'painters', 'Position', [700 200 900 600])
plot(RXheightFT,EIRxP,'k')
title('DME EIRxP vs Altitude')
ylabel('EIRxP (dBm)')
xlabel('Altitude (ft)')
grid on
```

APPENDIX G: ORIENTATION BASED CORRECTION MATLAB CODE

```
% --- Import Glide-Slope Pitch-Yaw Correction Factor ---
GSPitchYawCF = csvread('UASChamberMeas_Feb19.csv');
PITCH = [15 10 5 0 -5 -10 -15];
YAW = [-15 -10 -5 0 5 10 15];

% --- Import Channel Power Data for Correction (Glideslope Horizontal)
---
input = csvread('30cor1.csv');

% --- Subtract Glideslope Dipole Gain from Measurements ---
input(1,:) = input(1,:) - 0.55;

% --- Invert Pitch ---
input(3,:) = -1 * input(3,:);

% --- Normalization of GSPYCF ---
GSPitchYawCF = GSPitchYawCF - GSPitchYawCF(4,4);

% --- Mesh Plot ---
figure('Renderer', 'painters', 'Position', [700 200 900 600])
title('Normalized Glide-Slope Pitch-Yaw Correction Factor (dB)')
mesh(YAW,PITCH,GSPitchYawCF)
xlabel('yaw (degrees)')
ylabel('pitch (degrees)')

% --- Surface Plot ---
figure('Renderer', 'painters', 'Position', [700 200 900 600])
title('Normalized Glide-Slope Pitch-Yaw Correction Factor (dB)')
surf(YAW,PITCH,GSPitchYawCF)
xlabel('yaw (degrees)')
ylabel('pitch (degrees)')

% --- Interpolation ---
INTERSCALE = 50;
pitchHD = zeros(1,INTERSCALE*(length(PITCH)-1) +1);
yawHD = zeros(1,INTERSCALE*(length(YAW)-1) +1);
GSPitchYawCFHD = zeros(length(pitchHD));
pitchHD(end) = PITCH(end);
yawHD(end) = YAW(end);
for n = 1:(length(PITCH)-1)
    for m = 1:INTERSCALE
        pitchHD((INTERSCALE*(n-1)) + m) = PITCH(n) + (PITCH(n+1)-
PITCH(n))*((m-1)/INTERSCALE);
        yawHD((INTERSCALE*(n-1)) + m) = YAW(n) + (YAW(n+1)-YAW(n))*((m-
1)/INTERSCALE);
    end
end

for n = 1:length(YAW)
    GSPitchYawCFHD(((n-1)*INTERSCALE)+1,length(GSPitchYawCFHD)) =
GSPitchYawCF(n,length(GSPitchYawCF));
    for m = 0:(length(YAW)-2)
```

```
        for o = 0:(INTERSCALE-1)
            GSPitchYawCFHD(((n-1)*INTERSCALE)+1,(m*INTERSCALE)+o+1) =
GSPitchYawCF(n,m+1) + (GSPitchYawCF(n,m+2)-
GSPitchYawCF(n,m+1))*(o/INTERSCALE);
        end
    end
end

for n = 1:length(yawHD)
    for m = 0:(length(YAW)-2)
        for o = 1:(INTERSCALE-1)
            GSPitchYawCFHD((m*INTERSCALE)+1+o,n) =
GSPitchYawCFHD((m*INTERSCALE)+1,n) +
(GSPitchYawCFHD(((m+1)*INTERSCALE)+1,n)-
GSPitchYawCFHD((m*INTERSCALE)+1,n))*(o/INTERSCALE);
        end
    end
end

% --- Mesh Plot ---
figure
title('Interpolated Normalized Glide-Slope Pitch-Yaw Correction Factor
(dB)')
mesh(yawHD,pitchHD,GSPitchYawCFHD)
xlabel('yaw (degrees)')
ylabel('pitch (degrees)')

% --- Surface Plot ---
figure
title('Interpolated Normalized Glide-Slope Pitch-Yaw Correction Factor
(dB)')
surf(yawHD,pitchHD,GSPitchYawCFHD)
xlabel('yaw (degrees)')
ylabel('pitch (degrees)')

% --- Corrections to Channel Power ---
for n = 1:length(input)
    yawIndex(n) =
(round(input(2,n)*(INTERSCALE/5)))+((length(yawHD)+1)/2);
    pitchIndex(n) = ((length(pitchHD)+1)/2)-
(round(input(3,n)*(INTERSCALE/5)));
    corMeas(n) = input(1,n) -
GSPitchYawCFHD(pitchIndex(n),yawIndex(n));
end

% --- Plotting ---
figure('Renderer', 'painters', 'Position', [700 200 900 600])
plot(1:22,input(1,:),'-ok',1:22, corMeas(:),'--sk')
title('Glide-Slope Horizontal Sensitivity Channel Power')
legend('Pre-Correction','Post-Correction','location','southeast')
ylabel('dBm')
grid on

figure('Renderer', 'painters', 'Position', [700 200 900 600])
plot(1:22,input(2,:),'-ok')
title('Yaw')
```

```
ylabel('Degrees')
grid on

figure('Renderer', 'painters', 'Position', [700 200 900 600])
plot(1:22,input(3,:),'-ok')
title('Pitch')
ylabel('Degrees')
grid on

figure('Renderer', 'painters', 'Position', [700 200 900 600])
plot([-1 7],[0 0],'k',[0 2],[1 0],'k',[2 6],[0 2],'k',[0 2],[-1 0],'--
k')
ylim([-2 6])
xlim([-2 8])
```

VITA

Joseph Jantz

Candidate for the Degree of

Master of Science

Thesis: UNMANNED AERIAL SYSTEM INSPECTION OF ISTRUMENT LANDING SYSTEM RADIO SIGNALS

Major Field: Electrical Engineering

Biographical:

Education:

Completed the requirements for the Master of Science in Electrical Engineering at Oklahoma State University, Stillwater, Oklahoma in May 2019.

Completed the requirements for the Bachelor of Science in Electrical Engineering at Oklahoma State University, Stillwater, Oklahoma in 2017.

Experience:
Electrical Design Engineer, SubSite Electronics, Perry, OK (Jan 2019 – Present)
Graduate Research Assistant under Dr. Jim West, Oklahoma State University, Stillwater, OK (Jan 2018-May 2019)
Graduate Teaching Assistant, Oklahoma State University, Stillwater, OK (Fall 2018)
Electrical Engineering Intern, Frontier Electronic Systems, Stillwater, OK (Dec 2016 – Jan 2018)